Nivolumab Reaches Brain Lesions in Patients with Recurrent Glioblastoma and Induces T-cell Activity and Upregulation of Checkpoint Pathways

Signe K. Skadborg[1], Simone Maarup[2,3], Arianna Draghi[3], Annie Borch[1], Sille Hendriksen[1], Filip Mundt[4], Vilde Pedersen[2,7,8], Matthias Mann[4,9], Ib J. Christensen[2], Jane Skjøth-Ramussen[2,5], Christina W. Yde[6], Bjarne W. Kristensen[2,7,8], Hans S. Poulsen[2], Benedikte Hasselbalch[2], Inge M. Svane[3], Ulrik Lassen[2], and Sine R. Hadrup[1]

ABSTRACT

Glioblastoma (GBM) is an aggressive brain tumor with poor prognosis. Although immunotherapy is being explored as a potential treatment option for patients with GBM, it is unclear whether systemic immunotherapy can reach and modify the tumor microenvironment in the brain. We evaluated immune characteristics in patients receiving the anti-PD-1 immune checkpoint inhibitor nivolumab 1 week prior to surgery, compared with control patients receiving salvage resection without prior nivolumab treatment. We observed saturating levels of nivolumab bound to intratumorally and tissue-resident T cells in the brain, implicating saturating levels of nivolumab reaching brain tumors. Following nivolumab treatment, significant changes in T-cell activation and proliferation were observed in the tumor-resident T-cell population, and peripheral T cells upregulated chemokine receptors related to brain homing. A strong nivolumab-driven upregulation in compensatory checkpoint inhibition molecules, i.e., TIGIT, LAG-3, TIM-3, and CTLA-4, was observed, potentially counteracting the treatment effect. Finally, tumor-reactive tumor-infiltrating lymphocytes (TIL) were found in a subset of nivolumab-treated patients with prolonged survival, and neoantigen-reactive T cells were identified in both TILs and blood. This indicates a systemic response toward GBM in a subset of patients, which was further boosted by nivolumab, with T-cell responses toward tumor-derived neoantigens. Our study demonstrates that nivolumab does reach the GBM tumor lesion and enhances antitumor T-cell responses both intratumorally and systemically. However, various anti-inflammatory mechanisms mitigate the clinical efficacy of the anti-PD-1 treatment.

Introduction

At primary diagnosis, patients with glioblastoma (GBM) are treated with maximal surgery, radiation, and concomitant temozolomide, also known as Stupp's regimen (1). However, when relapse occurs, no standard treatment is available (2). Even though numerous treatment strategies have been explored, overall survival (OS) remains short at 14.6 months (1). Therefore, new treatment options are urgently needed, and immunotherapy is one strategy being explored that may show promise in selected patients (3, 4).

The brain is typically considered an immune-privileged organ, which has been equated with the notion that there is no passage of peripheral immune cells to the parenchyma of the brain (5). However, it has been shown that communication with the peripheral immune system does occur, including cellular exchange. It is known that T cells can be primed in the meningeal area of the brain (6). However, knowledge of the route of entry and presence of effector T cells in the parenchyma or tumor tissue localized in the brain is minimal. It has been shown in mice that cerebral spinal fluid (CSF) and interstitial fluid are drained via the central nervous system (CNS)-draining lymphatic vessels to the deep cervical lymph node, which suggests an alternative route for immune surveillance of the brain (7–9).

Immunotherapy has revolutionized cancer treatment, yet many cancer types are still unresponsive to current immunotherapeutic strategies (10–12). The effect of immune checkpoint inhibition has been sparse in GBM, and it has been questioned if the checkpoint inhibitors pass the blood–brain barrier (BBB) sufficiently to enter the tumor microenvironment (13). The anti-PD-1 immune checkpoint inhibitor nivolumab is a molecule of 146 kDa, whereas only molecules of 0.4 to 0.5 kDa are believed to pass the BBB freely (13). It has earlier been shown that the BBB is compromised in some

[1]Experimental and Translational Immunology, Department of Health Technology, Technical University of Denmark, Kongens Lyngby, Denmark. [2]Department of Oncology, DCCC Brain Tumor Center, Copenhagen University Hospital, Rigshospitalet, Copenhagen, Denmark. [3]National Center for Cancer Immune Therapy, CCIT-DK, Copenhagen University Hospital, Herlev, Denmark. [4]Novo Nordisk Foundation Center for Protein Research, CPR, University of Copenhagen, Copenhagen, Denmark. [5]Department of Neurosurgery, Copenhagen University Hospital, Rigshospitalet, Copenhagen, Denmark. [6]Center for Genomic Medicine, Copenhagen University Hospital, Rigshospitalet, Copenhagen, Denmark. [7]Department of Pathology, The Bartholin Institute, Copenhagen University Hospital, Rigshospitalet, Copenhagen, Denmark. [8]Department of Clinical Medicine and Biotech Research and Innovation Centre (BRIC), University of Copenhagen, Copenhagen, Denmark. [9]Research Department Proteomics and Signal Transduction, Max Planck Institute of Biochemistry, Martinsried, Germany.

S.K. Skadborg, S. Maarup, U. Lassen, and S.R. Hadrup contributed equally to this article.

Corresponding Author: Sine R. Hadrup, Department of Health Technology, Technical University of Denmark, Henrik Dams Allé, 204, 154, Kongens Lyngby 2800, Denmark. E-mail: sirha@dtu.dk

Cancer Immunol Res 2024;XX:XX–XX

doi: 10.1158/2326-6066.CIR-23-0959

areas of primary brain tumors, whereas other areas remain intact (14, 15). Additionally, some GBM tumors have high collagen levels, which can challenge the penetration capacity (16). Together, these characteristics may limit the penetrance of nivolumab and effector immune cells and hence compromise the effect of immunotherapy in GBM.

Checkpoint inhibitors have shown promising results in brain cancer in mouse models (17, 18), but such positive indications have not translated into treatment improvements in humans (19). Therefore, it is critical to determine if nivolumab sufficiently enters the brain and saturates PD-1 binding on T cells within GBM tumors. Here, we determined the effect of nivolumab treatment in a unique 7-day window of nivolumab treatment prior to surgical resection. We demonstrated the presence of nivolumab at saturated levels on tumor-resident T cells, even in this short treatment window. Furthermore, treatment mediated substantial changes in T-cell activation, proliferation, and checkpoint inhibition signatures, providing important clues to the minimal treatment effect and how to resolve this. Also, we found that T cells, both in blood and tumor, can recognize tumor-derived neoantigens, and these can be boosted by immunotherapy.

Methods and Materials

Trial design

CA209-9UP is an open-label phase 2 clinical trial, designed as a trial in a real-life setting to evaluate the treatment of recurrent GBM with nivolumab and bevacizumab under conditions close to routine practice (NCT03890952). In this study, Bristol Meyer Squibb sponsored nivolumab. At primary diagnosis, patients received Stupp's regimen (1). Patients were treated at Rigshospitalet, Copenhagen University Hospital, but the inclusion was open nationally upon transfer. In total, 44 patients were screened, where 4 were screen failures, leaving 40 patients that were included in the surgical group ($N = 20$) and non-surgical group ($N = 20$) depending on the possibility of salvage neurosurgical resection (**Fig. 1A**; Supplementary Fig. S1). All patients received 240 mg nivolumab and 10 mg/kg bevacizumab every 2 weeks. The surgical group also received 240 mg nivolumab approximately 7 days prior surgery. In total, 44 patients were included by January 2021, and follow-up ended in May 2022. End points were translational research, safety, and efficacy. The trial was approved by the Danish Ethical Committee (EudraCT 2017-003925-13), and written informed consents were obtained from patients with the possibility to withdraw consent at any time. The study was conducted in accordance with the Declaration of Helsinki and STROBE guidelines. Age at diagnosis, performance status, and multifocal disease at inclusion were registered. The extent of surgical resection was extracted from the operation note. Corticosteroid use was found in the record, medicine registry, or operation note. IDH1/IDH2 mutations were investigated by immunohistochemistry and next-generation sequencing. The cutoff value for O-6-methylguanine-DNA methyltransferase (MGMT status) methylated/unmethylated was 10%. Additional inclusion and exclusion criteria are listed in Supplementary Table S1. Additionally, control patients ($N = 10$) with recurrent GBM undergoing neurosurgical resection were included and donated fresh tumor tissue. The controls did not receive nivolumab or bevacizumab in the recurrent setting. Control patients provided written consent and followed our ethical guidelines according to Danish law. We used real-world data as controls from our GBM database on patients from Rigshospitalet, Copenhagen, and we found 156 patients treated with irinotecan and bevacizumab at recurrent setting from 2006 to 2014. Gender was equally distributed, and ages ranged from 23 to 79 years, with median age of 58 years. Of the 156 patients, 81 patients had salvage resection, whereas 75 patients had none. Clinical data from these patients were used as historical controls.

Statistical analyses and considerations of clinical results

The Kaplan–Meier method was used to estimate survival probabilities for OS as well as progression-free survival (PFS) for patients stratified by group with log rank statistics. Comparison of the patients in the trial to the historical controls was weighted using propensity scores based on age, gender, corticosteroid use, multifocal disease, MGMT status, and extent of resection. Separate analyses were conducted for those undergoing reoperation or not. Results were presented with 95% confidence limits, and the significance level was 5%. Calculations were done using SAS (v9.4, Cary). Multivariate analysis was performed using the Cox proportional hazards model with covariates: treatment group, gender, age per 10 years, MGMT status, and corticosteroid use.

Patient material

RNA/DNA extraction from tumor tissue or blood

Samples from tumors were available from the surgical group; recurrent tumor samples were collected and stored in RNAlater (Thermo Fischer Scientific) immediately after resection. Archival tissue from autologous primary tumor was available as fresh frozen tissue or formalin-fixed paraffin-embedded (FFPE) tissue. Blood samples for germline DNA were collected in Streck and EDTA vials. DNA and RNA were extracted from fresh frozen tissue using the AllPrep RNA/DNA/Protein Mini Kit (Qiagen). RNA was further DNase treated with RNeasy Mini Kit (Qiagen). DNA and RNA were extracted from FFPE slides by GeneRead DNA FFPE Kit (Qiagen) and Agencourt FormaPure Reagent Kit (Beckman Coulter), respectively. DNA from blood for germline whole-exome sequencing (WES) was extracted by ReliaPrep Large Volume HT gDNA Isolation System (Promega). Manufacturers' instructions were followed for all kits. Bioanalyzer 2100 with the 6000 RNA Nano and Pico Assay was used to evaluate the RNA quality. RNA was quantified using DeNovix spectrophotometer. DNA was quantified using Qubit Fluorometric Quantification (Thermo Fisher Scientific). Library preparation for WES was conducted by SureSelect Clinical Research Exome (Agilent). Library preparation for bulk RNAseq was performed using TruSeq Stranded Total RNA kit (Illumina) with unique dual indexes (UDI). Each sample was sequenced once and QC controlled to ensure >50× coverage for WES samples and >50 mill reads and >50% mRNA content for RNAseq. All sequencing was performed on NovaSeq 6000 (Illumina) using 2 × 150 bp paired-end sequencing.

Peripheral blood mononuclear cells (PBMC)

Peripheral blood samples were collected from patients at several time points (**Fig. 1A**): baseline (day 0, prior to treatment), after 8 weeks, and after 16 weeks. One additional blood sample was collected 3 weeks after nivolumab administration in the surgical group—2 weeks after surgery. PBMCs were isolated using Lymphoprep density gradient (Takeda) and cryopreserved in 10% DSMO (Herlev Hospital Pharmacy) and 90% human serum (Sigma-Aldrich/Merck KGaA) using controlled-rate freezing (CoolCells, BioCision) in −80°C and later stored in −140°C (**Fig. 1A**).

In vitro expansion of tumor-infiltrating lymphocytes

Minimally expanded young tumor-infiltrating lymphocytes (YTIL) were obtained from resected tumor tissue. In brief, tumor

tissue was cut into 1 to 3 mm^3 fragments and plated in wells of a 24 well-plate with 2 mL complete medium consisting of 90% RPMI-1640 plus GlutaMAX and 25 mmol/L N-2-hydroxyethylpiperazine-N-2-ethane sulfonic acid (HEPES; Gibco, Thermo Fisher Scientific), 10% heat-inactivated human AB serum (Sigma-Aldrich/Merck KGaA, Darmstadt, Germany), 100 U/mL penicillin, 100 μg/mL streptomycin (Pen/Strep, Gibco, Thermo Fisher Scientific), 1.25 μg/mL amphotericin B (Fungizone®, Bristol Myers Squibb), and 6,000 IU/mL of rhIL-2 (Proleukin®, Novartis). Plates were incubated at 37°C with 5% CO_2 and were inspected every other day from day 5 to investigate extrusion and proliferation of lymphocytes. Half of the medium was replaced with fresh complete medium every other day after day 5. Cells were split when needed, harvested after 3 to 6 weeks, and cryopreserved as described above (20, 21).

Rapid expansion protocol (REP) TILs were expanded from YTILs (just harvested or thawed). When biopsies were sparse, REP TILs were prioritized over young TILs because of a higher success rate in production of REP TILs than YTILs. Frozen YTILs were thawed and cultured in complete media for 48 hours prior to rapid expansion. During rapid expansion, 100,000 YTILs were cocultured with feeder cells and 30 ng/mL anti-CD3 (clone OKT3, Miltenyi Biotec) in 10 mL complete medium and 10 mL rapid expansion medium, which consisted of AIM-V (Thermo Fisher Scientific) and Fungizone® 1.25 μg/mL supplemented with 6,000 IU rhIL-2/mL in T25 flasks (Thermo Fischer Scientific). Feeder cells (PBMCs) from a minimum of six donors were thawed and irradiated by 40 Gy (Gammacell 3000 Elan, MDS Nordion). REP cultures were incubated at 37°C with 5% CO_2 for 5 days. On day 5 of the rapid expansion, half of the medium was replaced with 10 mL of mixed medium (consisting of 1:1 complete medium/rapid expansion medium). According to growth, the cultures were moved to larger flasks, and rapid expansion medium was added over the next 9 days. On day 14 + 1, REP TILs were harvested and cryopreserved as mentioned above (20, 21).

Tumor digest (single-cell suspension)

Fresh tumor samples from the operating theater were transported in a medium (RPMI-1640 plus GlutaMAX and 25 mmol/L HEPES; Gibco, Thermo Fisher Scientific) supplemented with Pen/Strep (Gibco, Thermo Fisher Scientific) on ice. The fresh tumor tissue was dissected under sterile conditions into fragments after the macroscopical vessels were removed. Tumor fragments were then placed in a T80 flask with 25 mL of digesting medium consisting of 100 mL RPMI-1640 plus GlutaMAX and 25 mmol/L HEPES supplemented with 1% Pen/Strep, 1 mg/mL collagenase (Cat. No C5138-100MG, Sigma-Aldrich), and 0.025 mg/mL dornase alfa (Pulmozyme®, Genentech) and placed overnight on a magnetic stirrer at room temperature. After a minimum of 18 hours, the digested tumor fragments were filtered through a 70 μmol/L filter to obtain a single-cell suspension. The single cells were cryopreserved as aforementioned.

An overview of the cell and tumor digest samples used in the study is shown in Supplementary Table S2.

Immunohistochemistry

FFPE GBM tissues from patients and controls were cut on a microtome (2 μm). The 10 controls had pathologically verified GBM and used a maximum of 20 mg prednisolone, comparable to the inclusion criteria in the trial. Tissue sections were deparaffinized and subject to heat-induced epitope retrieval with either Cell Conditioner 1 for 84 minutes at 100°C (CD3, PD-1, and IgG4) or EnVision TRS low pH for 40 minutes at 97°C (PD-L1). Endogenous peroxidase activity was blocked with EnVision FLEX Peroxidase-Blocking Reagent (Agilent Technologies). Incubation with CD3 ready-to-use (RTU) antibody (clone: 2GV6, Roche), PD-1 antibody (clone: MRQ22, Roche) diluted in EnVision FLEX Antibody Diluent K8006, and IgG4 antibody (clone: MRQ44, Cell Marque) diluted in the same diluent was performed using the BenchMark ULTRA Platform (Ventana Medical Systems) with the OptiView DAB IHC Detection system (Roche Diagnostics). Incubation with PD-L1 RTU antibody (clone: 22C3, Dako) was conducted using the Dako Omnis platform (Agilent Technologies) using the EnVision FLEX DAB^+ Chromogen (Dako Omnis) detection system. Nuclei were counterstained with hematoxylin. Unregistered fully anonymized human tonsil samples were used as controls and stained as above. Slides were evaluated using a BX51 microscope (Olympus Danmark A/S) and reviewed by the neuropathologist coauthor BWK. Slides were digitalized using the NanoZoomer XR digital image scanner.

Phenotyping by flow cytometry

Cryopreserved PBMCs, YTILs, REP TILs, and tumor digest were thawed and washed once in RPMI 1640 Medium with 10% fetal bovine serum (FBS, Gibco, Thermo Fisher Scientific) for cellular staining. Tumor digest was thawed and rested overnight in X-VIVO 15 (Lonza) with 5% heat-inactivated sterile filtered human serum (HS, Sigma-Aldrich) to regain surface marker expression after enzymatic digestion. PBMCs, YTILs, and REP TILs were thawed immediately before staining. PBMC and tumor digest were washed twice in PBS with 2% FBS (FACS buffer) and stained with a panel of fluorochrome-conjugated antibodies for surface markers (Supplementary Table S3 indicates the different panels of antibodies used for flow cytometry analysis) for 30 minutes (dark, 4°C), and cells were washed twice in FACS buffer. For staining of intracellular (ICS) markers in antibody panels B, C, and D, we used the eBioscience Foxp3/Transcription Factor Staining Buffer Set (Invitrogen) following the manufacturer's protocol. Fixation/permeabilization working solution was added to surface-stained PBMCs and tumor digest and incubated overnight (dark, 4°C). Cells were washed twice in 1× Permeabilization Buffer, antibodies for intracellular markers were added, and cells were stained for 30 minutes and hereafter washed twice with 1× Permeabilization Buffer. PBMCs and digest stained with panel A (surface markers only) were fixed in 1% PFA. Samples were resuspended in FACS buffer and acquired on an LSRFortessa (BD Biosciences). Phenotype analysis was performed once for each patient sample.

Analysis of flow cytometry data

Tumor digest contained much debris, and lymphocyte counts varied between patients. Samples with less than 30 events in the parent populations ($CD4^+$ T cells or $CD8^+$ T cells) were not included in the analysis. The number of events in parent population per patient samples is shown in Supplementary Fig. S2A. Flow cytometry data were analyzed in FlowJo v10.8.1. Manual gating was performed as depicted in Supplementary Fig. S2B.

TIL reactivity assay

YTILs and REP TILs were tested for reactivity against autologous tumor digest with cytokine intracellular staining. TILs were thawed in Pulmozyme buffer (RPMI-1640 plus GlutaMAX and 25 mmol/L HEPES; Gibco, Thermo Fisher Scientific) supplemented with Pen/Strep (Gibco, Thermo Fisher Scientific), 0.5 mL of magnesium

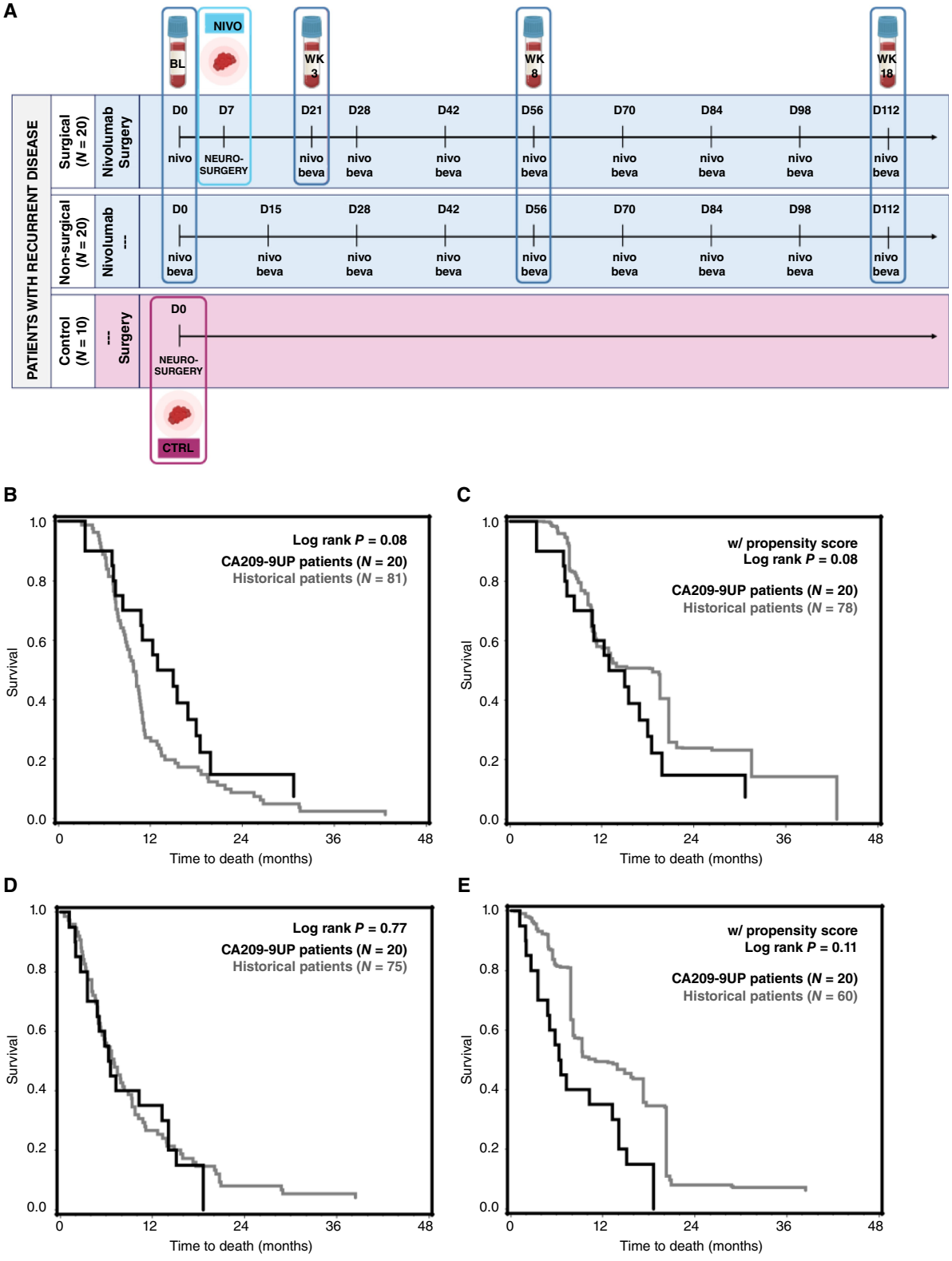

Figure 1.

Clinical setup and survival. **A,** Timeline showing administration of treatment with nivolumab (nivo) and bevacizumab (beva), including time points of sampling blood and tumor. Treated patients (blue) included a surgical group and nonsurgical group, and all patients received nivolumab and bevacizumab every 2 weeks. Patients in the surgical group also received nivolumab 7 days prior to surgery. Control (*Continued on the following page.*)

chloride (Herlev Hospital Pharmacy), and 0.025 mg/mL dornase alfa (Pulmozyme®, Genentech), and washed and cultured in RPMI$^+$ Pen/Strep$^+$ 10% HS with a concentration of 2 to 4 $\times$ 10^6 cells/mL. TILs were rested overnight at 37°C, 5% CO_2. Tumor digests were thawed in transport medium and washed. Cells from tumor digests were counted and resuspended in RPMI-1640$^+$ Pen/Strep$^+$ 10% HS at a concentration of 2 $\times$ 10^6 cells/mL. TILs were washed and resuspended in RPMI-1640$^+$ Pen/Strep$^+$ 10% HS at a concentration of 3 $\times$ 10^6 cells/mL. TILs and digest T cells were cocultured in a ratio of 3:1 by adding 100 µL TIL suspension and 50 µL autologous tumor digest suspension per well in a sterile 96-well plate (Thermo Scientific). GolgiPlug (BD Biosciences), GolgiStop (BD Biosciences), and anti-CD107a (BD Biosciences) were added according to the manufacturer's recommendations, and RPMI-1640$^+$ Pen/Strep$^+$ 10% HS was added up to a total volume of 200 µL per well. TILs stimulated with PMA/ionomycin (25 ng/0.5 µmol/L; Sigma-Aldrich/Sigma-Aldrich) or 0.4 µL Leukocyte Activation Cocktail (BD Biosciences) were used as positive controls. TILs alone were used as negative controls. Melanoma or colorectal carcinoma tumor cell lines without MHC-I and MHC-II expressions because of *B2M* or *CIITA* knockout by CRISPR-associated protein 9 (CAS9) were additionally used as negative controls, both previously described (see "Control tumor cell lines"; refs. 20, 22). The cocultures were incubated for 8 hours in a humidified incubator 37°C with 5% CO_2 and then stained as described above (see "Phenotyping by flow cytometry") using antibody panels C or D (Supplementary Table S3). Stained cells were acquired on an LSRFortessa or NovoCyte Quanteon Flow Cytometer (Agilent) and analyzed with FlowJo 10.6.1 or 10.8.1. Reactivity assays were repeated for verification of results.

Control tumor cell lines

Short-term (<10 passages) *in vitro* cultured tumor cell lines were established via serial passage of adherent cells from tumor fragments in RPMI-1640 plus GlutaMAX and 25 mmol/L HEPES (Cat. No 72400-021, Gibco, Thermo Fisher Scientific) supplemented with Pen/Strep, 10% FBS (Cat. No 10270106, Gibco, Thermo Fisher Scientific), and 500 ng/mL of hydrocortisone (Solu-Cortef®, Pfizer). All tumor cell lines were generated internally and authenticated via *in vitro* patterns of growth, morphology (light microscopy), and, when in doubt, expression of lineage antigens by PCR. Mycoplasma testing (Cat. No A3744.0020, VWR International) was routinely performed according to the manufacturer's instructions. No *Mycoplasma* infection was detected in the past 6 years. Established tumor cells were cultured in RPMI-1640 plus GlutaMAX and 25 mmol/L HEPES supplemented with Pen/Strep and 10% of FBS. To abrogate the expression of MHC molecules, the tumor cell lines were subjected to CRISPR-Cas9-mediated knockout of *B2M* or *CIITA*, as previously described in detail (22). crRNAs targeting the *B2M* (5′- CAGTAA GTCAACTTCAATGT-3′) and *CIITA* (5′-GATATTGGCATAAGC CTCCC-3′) genes were selected from the literature (23) or designed using the Custom Alt-R® CRISPR-Cas9 guide RNA design tool (Integrated DNA Technologies). sgRNAs and S.p. HiFi Cas9 Nuclease V3 were purchased from Integrated DNA Technologies' Alt-R catalog, and ribonucleoprotein (RNP) complexes were formed as per the manufacturer's instructions. Approximately 40,000 tumor cells were then seeded in a well of a 96-well plate with flat bottom and transfected with RNP complexes at a concentration of 10 nmol/L using Lipofectamine CRISPRMAX Cas9 Transfection Reagent (Cat. No CMAX00008, Thermo Fisher Scientific) following the manufacturer's instructions. After at least 72 hours, the cells were treated for additional 72 hours with 100 IU/mL IFNg (Cat. No 300-02, Peprotech) to induce MHC molecules upregulation. The loss of MHC molecules expression was verified by flow cytometry. Purified *B2M* KO and *CIITA* KO populations were generated by electronic sorting on a BD FACS Melody Cell Sorter (BD Biosciences) and further expanded. In the experiments performed in this study, the purified populations were further cultured before testing for less than 2 months or a maximum of 10 additional passages.

Transcriptomics

Preprocessing of the RNA sequencing FASTQ files was done using trimming with TrimGalore 0.6.4 (24), which was combined with Cutadapt (25) and FastQC version 0.11.9 (26). Kallisto quant version 0.46.0 (27) was used to align the trimmed reads to GRCh38 (28). The kallisto output was used as input to estimate the cell population with the Microenvironment Cell Population counter (MCP-counter) version 1.2.0 (https://genomebiology.biomedcentral.com/articles/10.1186/s13059-016-1070-5).

Proteomic analyses

Sample preparation for mass spectrometry-based analyses

Frozen tumor tissue were processed by Qiagen© AllPrep DNA/RNA/Protein Mini Kit for protein purification. The final flow-through containing the proteins was processed through acetone precipitation as previously described (bioRxiv 2023.05.12.540582). The resulting protein pellet was resuspended in 200 µL, 8 mol/L urea, in Tris-HCl (pH 8.0), supplemented with PhosSTOP (Roche) and Complete Protease Inhibitor (Sigma-Aldrich), following the manufacturer's instructions. The pellet was completely dissolved by pipetting and sonication (Bioruptor®, Diagenode; 5 times 30 seconds on and 30 seconds off cycles). Protein concentrations were determined, and protein solutions were reduced and alkylated as described, followed by tryptic digest and peptide cleanup on two 14-gauge styrene divinylbenzene reverse-phase sulfonate StageTip plugs using a previously described protocol (bioRxiv 2023.05.12.540582, 29). Clean peptides were resuspended in 10 µL 0.1% formic acid and analyzed on a NanoDrop for their concentrations as before.

Mass spectrometry analyses

A total of 200 ng clean peptides were loaded on C18 Evotips (Evosep) following the manufacturer's protocol. Briefly, tips were

(*Continued*.) patients (purple) with recurrent glioblastoma undergoing neurosurgical resection were additionally included. These patients did not receive nivolumab before resection. Additionally, blood samples were collected from treated patients at day 0 as baseline (BL), after 8 weeks (WK 8), and at 16 weeks (WK 16). An additional blood sample was collected from patients in surgical group 3 weeks (WK 3) after nivolumab administration (2 weeks after surgery). **B–E,** Overall survival by Kaplan–Meier curves comparing patients in our CA209-9UP clinical trial ($N = 40$, black line) with a historical patient group ($N = 156$, grey line) from our one-site database, who were treated with bevacizumab and irinotecan from 2006 to 2014 but not nivolumab. All patients were subdivided into (**B** and **C**) a surgical group and (**D** and **E**) a nonsurgical group. Comparison between the historical patient group and the patient in trial was done (**B–D**) without using propensity scores and (**C–E**) weighted using propensity scores based on age, gender, corticosteroid use, multifocal disease, MGMT status, and extent of resection.

wetted in isopropanol for 10 seconds and then activated with 20 μL 100% acetonitrile with 1% formic acid. Evotips were cleared by 1 minute centrifugation at 800 round centrifugal force (rcf) and again wetted in isopropanol for 10 seconds. The Evotips were then conditioned with 20 μL of 0.1% formic acid and cleared for 1 minute at 800 rcf before 200 ng of samples was loaded and spun down (800 rcf for 1 minute). We loaded a total of 300 ng of desalted peptides per sample on each tip. Tips were then washed once with 20 μL of 0.1% formic acid and centrifuged at 800 rcf for 1 minute, before being stored with 100 μL of 0.1% formic acid on the tips and plenty of 0.1% formic acid in the Evotips box to prevent drying. The charged tips were loaded on a One liquid chromatographer (Evosep) and injected at a rate of 30 samples per day, i.e., with a 44-minute gradient. Samples were analyzed on a timsTOF Pro (Bruker) using diaPASEF acquisition mode. The column used was commercially prepacked with 1.5 μm C18-beads (PepSep) with the following dimensions: 15 cm × 150 μm inner diameter. The column was heated to 40°C during the runs. For reference of the original diaPASEF method, please see Meier and colleagues (30). Mass spectrometry diaPASEF raw files were searched with DIA-NN software (version 1.8). Samples were searched against the human FAST files (9606), which were *in silico* digested for library free searches and library generation. Missed cleavages were set to 1, and the number of allowed variable modifications was set to 2. N-terminal methionine excision, cysteines carbamidomethylation, methionine oxidation, and N-terminal acetylation were selected as modifications. Peptide lengths were allowed within, and including, 7 to 30 amino acid residues. Precursor charge range was set to 2 to 4, precursor m/z ranges from 100 to 1,700, and fragment ion m/z ranges from 200 to 1,800. Mass accuracy and MS1 accuracy were both set to 15.0, matches between runs were enabled, and likely interferences were removed. Data were researched in a second pass using the on-the-fly generated spectral library. For more details, see DOI: https://doi.org/10.1101/2023.05.12.540582 (bioRxiv 2023.05.12.540582). Data were $\log_2$-transformed and median absolute deviation (MAD) normalized (robust z-scores) before bioinformatical analyses.

Differential expression analysis

Differential expression analysis (DEA) for proteomics and transcriptomics was performed with DeSeq2 version 1.30.1 (31). The results with genes and log-fold change were used as input to a Gene Set Enrichment Analysis (GSEA) with clusterprofiler packages from R version 4.2.2 (32), and both the Gene Ontology (GO) database and Kyoto Encyclopedia of Genes and Genomes (KEGG) database were applied. Complexity heatmap version 2.10 (33) was used for the heatmap, and enriched figures were made with geasqplot2 from enrichplot (34).

Detection of neoantigen-reactive T cells in PBMCs and TILs

Neoantigens were predicted from the WES data. The mutations were detected by the GATK4 best practice (35). Firstly, the WES reads were trimmed using TrimGalore 0.6.4 (24) combined with Cutadapt (25) and FastQC 0.11.9 (26) with a minimum length of 50 bp and other default settings. The trimmed reads were aligned to the human reference genome, GRCh38 (28), using BWA-MEM 0.7.16a (36), followed by the preprocessing steps including MarkDuplicate and base re-calibrator (35). Somatic variant calling was performed using MuTect2 (37), with filtering of panel of normal (PON) and contamination filter from GTAK best practice. MuPeXI (38) was used to predict neoepitope candidates, which were filtered by the expression of the corresponding gene obtained from kallisto version 0.46.0 (27) and the binding to the corresponding HLA-allele predicted with NetMHCpan 4.1 (39). The patient-specific HLA alleles were typed using Razers3 (version 3.4; ref. 40) followed by OptiType version 1.2 (41). The criteria for selecting neoepitope candidates were expression level ≥0.1 TPM and then the top 100 of the best EL % Rank to the HLA allele but only including HLA binders. Neoantigens were predicted for both primary and recurrent tumors.

PBMCs, YTILs, and REP TILs were screened once for neoantigen-reactive $CD8^+$ T cells (NART) and virus antigen-reactive T cells (VART) using in-house assembled DNA barcode-labelled peptide-MHC-I (pMHC) multimers (42). In short, DNA barcode-labelled peptide-MHC-I multimers were assembled so each DNA barcode was specific for each pMHC in the neoantigen panel (Supplementary Table S4). The multimers were built on a streptavidin-conjugated dextran backbone labelled with a fluorochrome (NARTs: PE, VARTs: APC; FINA Biosolutions LLC). Predicted neoantigen peptides (Pepscan) were loaded in their respective biotinylated MHC monomers (produced in-house). Biotinylated DNA barcodes (produced in-house) and biotinylated pMHC were bound to the fluorochrome-conjugated dextran backbone via the streptavidin binding sites. Patient samples were stained with a patient-specific pool of pMHC multimers, together with CD8 and CD3 antibodies (Supplementary Table S3). PE- and APC-labelled $CD8^+$ T cells were then sorted by fluorescence activating cell sorting (FACS) on FACSAria (BD Biosciences). DNA barcodes in the sorted cells were then amplified by PCR. A baseline sample from the multimer pool was also amplified as a reference. PCR products were sequenced by PrimBio, and sequencing results were analyzed in Barracoda. Production and downstream application of DNA barcoded-labelled pMHC multimers are thoroughly described by Bentzen and colleagues (42). Output files from Barracoda included information on the fold change of enriched DNA barcodes in the sorted samples compared with the baseline and whether the enrichment was significant. A fold change ($\log_2$) over 2 and $P < 0.001$ were set as thresholds for a significantly enriched DNA barcode, at which point the T-cell recognition of the pMHC was annotated.

Verification peptide reactivity

Peptides detected by NARTs were verified by peptide-specific expansion of patient PBMCs. PBMCs were cocultured with a pool of reactive peptides for 14 days. PBMCs were cultured in X-VIVO (Lonza) with 5% human serum. Peptides were added at day 0 with a concentration of 10 μg/mL per peptide. PBMCs were additionally stimulated with 40 IU/mL IL2 and 0.5 μg/mL purified anti-CD28 (BD Biosciences, clone: CD28.2). The medium with IL2 was changed twice per week. To validate the pMHC specificity of the given T-cell cultures, PBMCs expanded with peptides were stained with single tetramers produced in-house. Approximately 400 μmol/L DMSO-dissolved peptides (Pepscan) were mixed with in their respective biotinylated MHC monomers [produced in-house (42)] with a concentration of 200 μg/mL in a 1:1 volume resulting in final concentrations of 200 μmol/L peptides and 100 μg/mL MHC monomers. Peptide exchange is performed via UV radiation (366 nm) for 1 hour. The pMHCs are hereafter mixed with fluorochrome-conjugated streptavidin (final concentration 0.018 μg/μL, PE and APC, BioLegend) and hereafter incubated for 30 minutes on ice in the dark. Approximately 0.056 μL 500 μmol/L D-biotin (Avidity) or 1 μL pMHC-streptavidin product and 10× freezing buffer (PBS with 5% BSA, Sigma-Aldrich, and 50% glycerol, Sigma-Aldrich) was added, and tetramers were hereafter stored at −20 degrees. For staining of PBMCs, each tetramer

was fluorochrome labelled with PE and APC. Expanded PBMCs were washed twice in FACS buffer and hereafter stained with 2 μL tetramer (1 μL APC conjugates and 1 μL PE conjugates), and PBS was added up to a total staining volume of 80 μL. PBMCs were incubated for 15 minutes at 37°C in the dark. Approximately 20 μL Ab mix containing CD3-FITC, CD8-BV480, CD4-BUV394, and NiR (See Supplementary Table S3 for information) was added and incubated on ice for 30 minutes in the dark. The samples were washed twice in FACS buffer and were analyzed using an LSRFortessa (BD Biosciences) and FlowJo v10.

Statistical analysis

For bar plots, unpaired *t* test was used to compare the means of two groups and performed with a 95% confidence interval. *, $P < 0.05$; **, $P < 0.01$; ***, $P < 0.001$; ****, $P < 0.0001$. Other statistical analyses are described in detail in the given method section.

Data availability

The data generated in this study are available within the article and its supplementary data files or can be obtained from the corresponding author upon reasonable request. Raw patient data cannot be shared freely because of the constraints of the informed consent and regulations stipulated by Danish and EU laws. Each request for data use must undergo assessment and validation to ensure compliance with the consent and legal provisions. Raw sequencing data is stored at the Danish National Genome Center and can be shared upon appropriate data access agreement. The Danish National Genome Center has provided an online guide for applying for data access, available at https://www.eng.ngc.dk/research-and-international-collaboration/dngc-research-services/how-to-apply-for-access. Patient IDs used in the study can be obtained from the authors, following the data access application.

Results

Tumor and peripheral blood were collected to analyze nivolumab's immune effects in patients with GBM

CA209-9UP is an open-label phase 2 clinical study, in which 44 patients with recurrent GBM following Stupp's regimen (1) were included from November 2018 to January 2022. Four patients became screen failures, whereas 40 patients were treated with nivolumab (PD-1 inhibitor) and bevacizumab (anti-VEGF-A) every 14 days. The patients were divided in two groups; 20 patients received a first dose of 240 mg nivolumab 7 days before salvage resection as a window of opportunity to study treatment effects in tumor tissue (surgical group), whereas 20 patients were considered nonoperable (nonsurgical group; **Fig. 1A**; Supplementary Fig. S1). Additionally, we included 10 control patients with recurrent GBM, not treated with nivolumab or bevacizumab, to investigate if nivolumab could influence the immune cellular signatures at the tumor site in recurrent patients with GBM (**Fig. 1A**). Tumor and blood samples were collected as illustrated in **Fig. 1A**.

Nivolumab and bevacizumab treatment provide no apparent survival benefit for patients with GBM

The 40 patients included in the CA209-9UP clinical trial for evaluation of nivolumab and bevacizumab treatment had a median age at diagnosis of 57.5 years (surgical group) and 50.5 years (nonsurgical group). For both patient groups, 77% (31 out of 40 patients) did not receive corticosteroids at inclusion (Supplementary Table S5). The 10 control patients had a median age of 57 years, and 90% of the control patients did not receive corticosteroids at inclusion (1 out of 10 patients; Supplementary Table S5). Tumor samples were historically verified as GBM; however, today, eight CA209-9UP patients (three surgical and five nonsurgical group) and two controls would classify as astrocytoma, IDH-mutant, WHO grade IV according to WHO's recent classification of brain tumors (2, 43). The tumor classification changed in 2021 after the onset of this clinical trial. The patient groups had equal distributions of gender, performance status, and corticosteroid usage, whereas 45% of patients in the surgical group harbored unmethylated MGMT compared with 55% in the nonsurgical group. Fewer of the control patients were MGMT unmethylated (20%), and more had a total resection (90%), whereas the extent of disease was similar to the CA209-9UP patients (Supplementary Table S5). Overall, the treatment was well tolerated. One suspected unexpected serious adverse reaction (SUSAR) of posterior reversible encephalopathy syndrome (PRES) was reported, and the patient was excluded from further treatment. Serious adverse events of grades 3 and 4 (CTCAE version 4.03) are listed in Supplementary Table S6.

For all patients in CA209-9UP, we observed a median overall survival (mOS) of 10.9 months (7.0–14.1) and median progression-free survival (mPFS) of 4.1 months (3.8–5.9). When stratified, the surgical and nonsurgical groups had an mPFS of 6.0 and 3.8 months, respectively, and an mOS of 14.0 and 6.4 months, respectively. mOS follow-up was 30.0 months (15.2–40.1) and 27.2 months (16.0–41.0) in the surgical and nonsurgical groups, respectively. Multivariate analysis was performed by the following variables: corticosteroid use, MGMT status, gender, age at diagnosis, and treatment group (Supplementary Table S7). Corticosteroid use at inclusion was a significant negative predictor of outcome ($P = 0.04$). In a follow-up survival analysis, we removed these patients, but no difference was observed, compared with the results from the whole group. We then stratified on the differences in corticosteroid use at baseline ($N = 40$) and saw that corticosteroid-using patients had mOS of 7.3 months compared with noncorticosteroid-using patients with mOS of 12.2 months.

To evaluate the potential effect of nivolumab and bevacizumab treatment, real-world data on the historical patient group was extracted from our one-site GBM database, from which we have reported before (44). Using real-world data as controls is an established method that has previously been used (45). The historical patient group comprised patients treated with bevacizumab and irinotecan and possibly neurosurgical resection ($N = 156$; 81 patients had a neurosurgical resection, whereas 75 patients did not). The historical surgical group ($N = 81$) had an mOS of 9.8 months, compared with the mOS of 14.0 months in our nivolumab/bevacizumab-treated surgical patient group. Although a marginal difference was initially observed between the two groups (log-rank of $P = 0.08$; **Fig. 1B**), no difference was observed (log-rank *P*-value = 0.46; **Fig. 1C**) when the patient cohorts were matched based on propensity scores, including relevant clinical and performance characteristic. In the nonsurgical group, matched historical patients ($N = 75$) had an mOS of 7.0 months, whereas the nivolumab/bevacizumab-treated patient group had an mOS of 6.4 months. Hence, no difference was observed, neither without nor with matching based on propensity score (log-rank of $P = 0.77$ and $P = 0.11$, respectively; **Fig. 1D** and **E**).

When comparing survival (PFS and OS from recurrence) of the surgical group (NIVO) to control patients used for immunological analyses, no difference in survival was observed (Supplementary Fig. S3). In conclusion, we found no survival benefit among patients

treated with nivolumab and bevacizumab compared with matched historical patients. However, we did observe five long-term survival patients (>20 months after tumor recurrence) in the nivolumab/bevacizumab-treated group. The length of survival was unexpected based on clinical parameters, such as time from primary diagnosis to progression (4.8, 6.7, 4.9, 14.8, and 8.7 months) and MGMT or IDH status (two MGMT unmethylated, one IDH mutated), and hence may indicate clinical effect of nivolumab treatment in selected cases.

Nivolumab can be found in GMB brain lesions and saturates PD-1 expressed on intratumoral T cells

Tumor samples were analyzed to evaluate if nivolumab can penetrate to the brain and reach the tumor site in sufficient amount to saturate PD-1 binding on T cells. To detect nivolumab binding to PD-1 on T-cell surfaces, we applied a fluorochrome-conjugated anti-IgG4, the isotype of nivolumab, whereas free PD-1 molecules were determined by a regular fluorochrome-conjugated anti-PD-1 (**Fig. 2A**). Tumor digests were rested overnight to reexpress certain T-cell surface markers lost during tissue digestion. Before rest, T cells were only binding anti-IgG4, indicating all PD-1 molecules were bound to nivolumab. After rest, T cells bound both anti-PD-1 and anti-IgG4, indicating surface presence of new PD-1 molecules during the resting period or loss of nivolumab binding. Intratumoral T cells from control patients only bound anti-PD-1, confirming that IgG4 binding is specific to nivolumab and the PD-1 molecules on unrested T cells were intact after the enzymatic digestion (**Fig. 2B** and **C**). Together, this demonstrates that surface-expressed PD-1 on intratumoral T cells is fully saturated with nivolumab after only 7 days of treatment and that nivolumab must be present in an unbound form in the tumor microenvironment to capture recent surface mobilized PD-1.

Tumor digests were stained for CD69 and CD103, markers that when co-expressed identify tissue residency, to determine whether T cells in the tumor digest included tissue-resident T cells. Both markers were expressed on both $CD4^+$ and $CD8^+$ T cells in the tumor digest, with no difference in frequencies between NIVO and control patients (**Fig. 2D**). A large fraction of the tissue-resident CD103 and CD69 co-expressing T cells were also saturated for nivolumab binding, exclusively in the treated patients (**Fig. 2E–F**). This further supports the notion that nivolumab enters the GBM lesion primarily as free molecules, and any contribution from peripheral T cells binding to nivolumab and migrating to the tumor is minimal.

We also performed single staining for CD3, PD-1, and IgG4 of consecutive paired FFPE slides from primary and recurrent NIVO tumors. In this analysis, three patients were identified with distinct $PD\text{-}1^+$ and $IgG4^+$ cells in the recurrent tumors after nivolumab treatment, whereas FFPE sections from the corresponding untreated primary tumors were $IgG4^-$ (Supplementary Fig. S4). Despite not being able to perform multicolor staining of the FFPE slides, these data support our results obtained in the flow cytometry-based analysis of tumor digest.

Altogether, this suggests that nivolumab entered the brain lesions and penetrated the tumor tissue as free immunoglobulins, in sufficient levels to saturate PD-1 expression on intratumoral T cells, only 7 days after administration.

Nivolumab mediates CNS homing and profound T-cell activation in GBM

After establishing that nivolumab penetrated the GBM tissue, we evaluated the influence on T-cell composition and signatures in NIVO patients compared with the control patients. No overall differences in the frequencies of $CD4^+$ and $CD8^+$ T cells within the T-cell compartment were observed between the two groups (**Fig. 3A**). Additionally, when looking into the overall immune cell representation [including T cells, B cells, fibroblasts, monocyte lineage cells, myeloid dendritic cells (mDC), etc.] using the MCP-counter tool to analyze transcriptomic data, no difference was found between NIVO and control patients (Supplementary Fig. S5A).

We further examined T-cell expression of markers related to migration, activation, and late differentiation using multicolor flow cytometry. The chemokine receptors CD183 (CXCR3) and CD195 (CCR5) have previously been correlated with CNS homing in neurological inflammation (46, 47). With inflammation considered a hallmark of cancer (48), we investigated the expression of these two chemokine receptors. The frequency of $CD4^+$ T cells co-expressing CD183 and CD195 was higher in nivolumab-treated tumors compared with controls, whereas it is stable for $CD8^+$ T cells (**Fig. 3B**). Furthermore, a significant increase in frequency of T cells expressing high levels of CD183 and CD195 was found on $CD4^+$, and the same tendency was observed among $CD8^+$ T cells in tumors of NIVO patients compared with control patients. Increased expression of these chemokine receptors suggests a treatment-related effect (**Fig. 3C** and **D**). An example of gating for T cells expressing higher levels of chemokine receptors is shown in **Fig. 3E**. This coincided with a trend toward lower frequencies of both $CD4^+$ and $CD8^+$ T cells co-expressing these chemokine receptors in peripheral blood (Supplementary Fig. S6). Together, this suggests that nivolumab can reinforce CNS T-cell recruitment. When looking into peripheral T cells in the entire nivolumab/bevacizumab-treated patient cohort, we found that PBMCs from the nonsurgical group had significantly higher frequencies of $CD183^+CD195^+$ T cells within the $CD8^+$ T-cell population at baseline (day 0) and week 16 compared with the surgical group (**Fig. 3F**). The larger fraction of cells with this migratory phenotype suggests a more pronounced neurological inflammation in patients where the tumor is maintained and hence directly affected by the tumor milieu. Finally, a high frequency of T-cell co-expression of CD183 and CD195 also positively correlated with the MCP-counter score for mDCs, which could be responsible for the recruitment of T cells (Supplementary Fig. S5B).

As we found a CNS homing signature among T cells in both blood and tumor, we further evaluated the activation status of intratumoral T cells after nivolumab treatment. A significantly enhanced proliferation was observed among both intratumoral $CD8^+$ and $CD4^+$ T cells following nivolumab treatment, based on the detection of Ki67 expression (**Fig. 3G**). Furthermore, the frequency of T cells expressing the co-stimulatory molecule CD28 did not change significantly following treatment (**Fig. 3H**), but patients with a higher frequency of $CD8^+$ T cells expressing CD28 tended to have longer PFS and OS after recurrence but only among NIVO patients (Supplementary Fig. S7), suggesting that co-stimulation might influence T-cell behavior in nivolumab -treated patients.

Among the tissue-resident T cells expressing CD103 and CD69, the co-expression of CD39, a marker of recent T-cell activation, was only observed among NIVO patients (**Fig. 3I**; Supplementary Fig. S6). A similar tendency was found within $CD4^+$ T cells but at a much lower frequency level (**Fig. 3H**). Furthermore, the expression of the early activation marker CD137 (4-1BB) tended to increase in tissue-resident $CD8^+$ T cells after nivolumab treatment (**Fig. 3J**).

Signatures of immune modulation were likewise apparent from transcriptomic data obtained from resected tumor material of the NIVO and control groups. From a DEA, genes related to inflammation, including *FOXA* and *CXCL17*, and *FGFBP2*, a gene related to T-cell effector function, were significantly overexpressed in the NIVO group. However, most other significantly overexpressed genes were

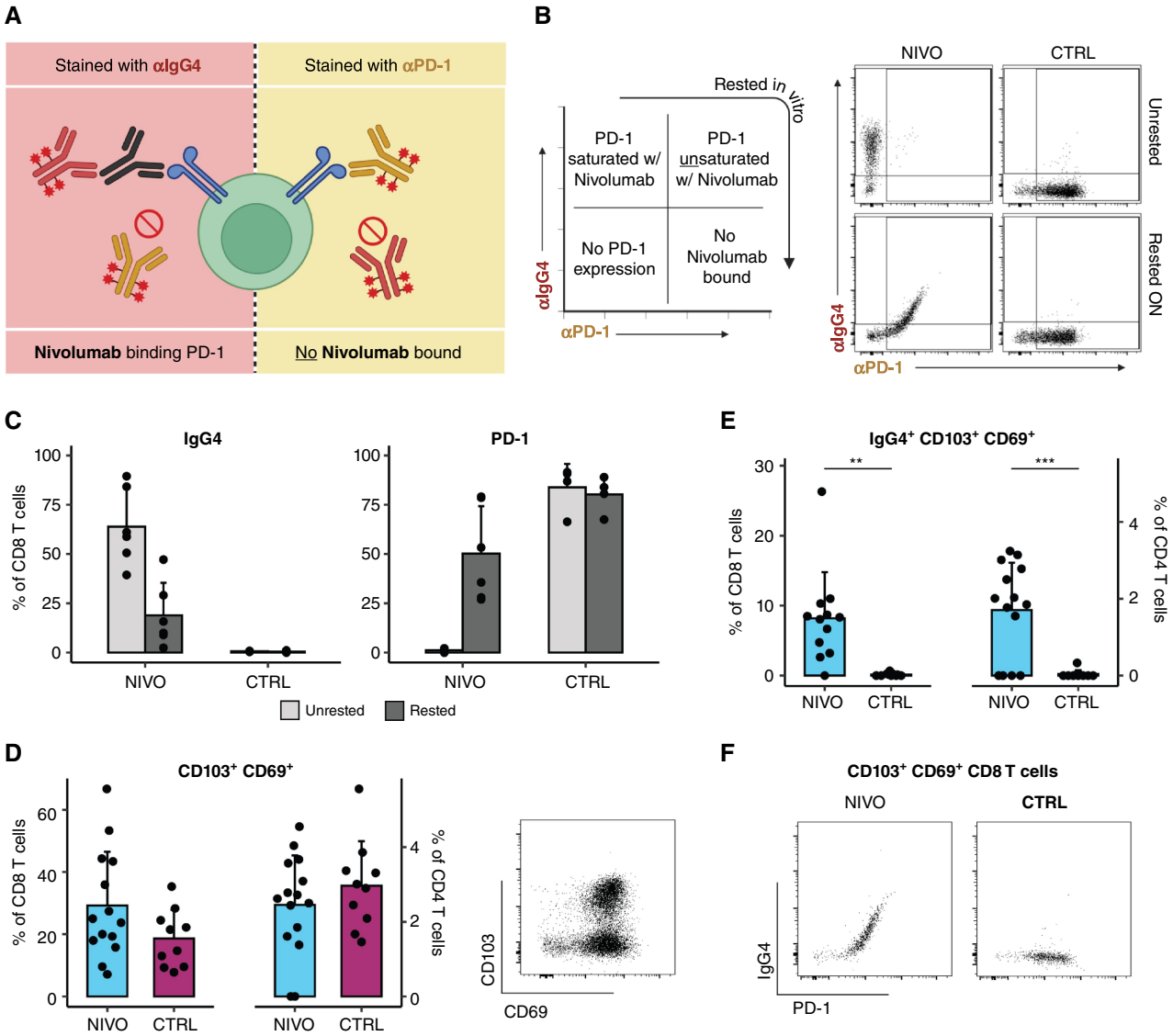

Figure 2.

Intratumoral detection of nivolumab and tissue-resident T cells. **A,** Illustrative explanation of PD-1 and nivolumab antibody (Ab) detection; nivolumab bound to PD-1 was detected with a fluorochrome-conjugated anti-IgG4 Ab (red) binding to the Fc region of nivolumab (black Ab), whereas free PD-1 molecules were detected with fluorochrome-labelled anti-PD-1 Ab (yellow) by flow cytometry. **B,** Explanation of dot plots showing nivolumab binding and saturation (left) and representative flow cytometry dot plots of unrested and rested tumor digest stained with anti-PD-1 and anti-IgG4, showing a complete nivolumab saturation of intratumoral T cells in unrested tumor digest from nivolumab-treated (NIVO) patient, which is partly lost after resting. Intratumoral T cells from control (CTRL) patients do not bind anti-IgG4 (right). **C,** Frequency of $CD8^+$ T cells stained with anti-IgG4 (nivolumab bound) and anti-PD-1 (free PD-1 molecules) in unrested (light gray) and rested (dark gray) tumor digest (NIVO $N = 6$; CTRL $N = 4$). **D,** Frequency of $CD8^+$ and $CD4^+$ T cells co-expressing the markers of tissue residency, CD69 and CD103, in tumor digest from NIVO patients (light blue; CD8 NIVO $N = 14$; CD4 NIVO $N = 15$) and CTRL patients (purple; CD8 CTRL $N = 10$; CD4 CTRL $N = 10$; left). Representative plot of intratumoral $CD8^+$ T cells expressing CD69 and CD103 (right). **E,** Frequency of $CD8^+$ and $CD4^+$ T cells binding nivolumab (anti-IgG4) that are tissue-resident T cells (CD8 NIVO $N = 12$; CD8 CTRL $N = 10$; CD4 NIVO $N = 14$; CD4 CTRL $N = 10$). **F,** Representative plots from NIVO and CTRL patients showing tissue-resident $CD8^+$ T cells from rested tumor digest binding anti-PD-1 and anti-IgG4. For bar plots indicated, the mean and error bars show SD. Means were compared between NIVO and CTRL using unpaired *t* test. *, $P < 0.05$; **, $P < 0.01$; ***, $P < 0.001$; ****, $P < 0.0001$.

related to cancer progression (*MT-RNR1*, *SNORA7A*, *MIR663B*, *MIR6087*, *FGG*, *FGA*, *HMGCS2*, *PIP*, *REG1A*) rather than immune response signatures (**Fig. 3K**; Supplementary Fig. S8).

Taken together, a profound signature of T-cell activation and proliferation was observed in GBM tumors 7 days after nivolumab treatment.

Nivolumab treatment induces strong compensatory upregulation of immune inhibitory pathways

In addition to the T-cell activation signature observed following nivolumab treatment, upregulation of co-inhibitory molecules was identified. Significantly higher frequencies of both $CD8^+$ and $CD4^+$ T cells expressing TIGIT, LAG-3, TIM-3 ($CD8^+$), and CTLA-4 were

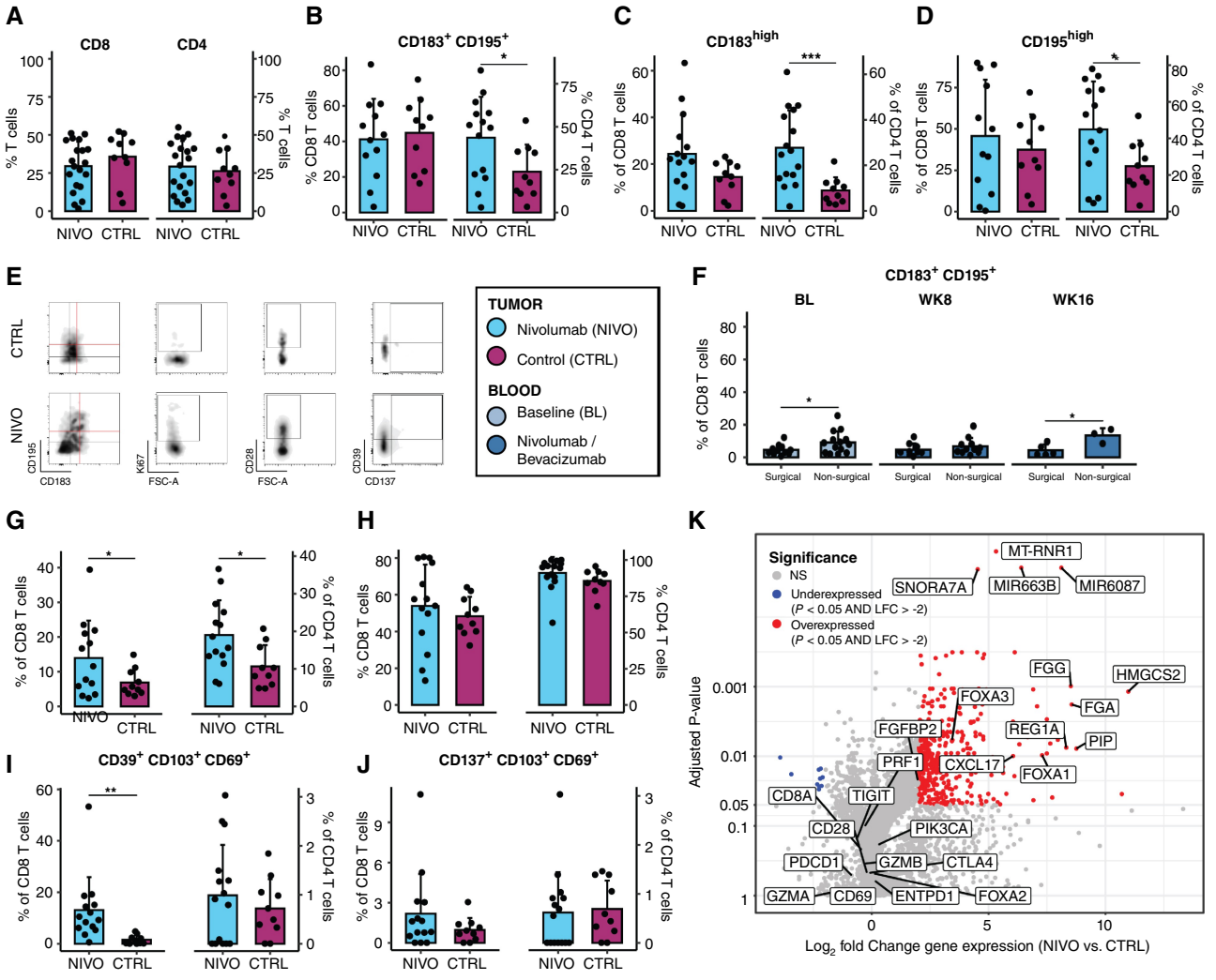

Figure 3.

CNS homing, activation, and proliferation in tumor tissue and blood. **A–J,** The frequency of intratumoral T cells expressing different markers for migration, activation, and proliferation was detected by flow cytometry to compare the distribution of these within the GBM tumor of nivolumab-treated patients and control patients. **A,** Firstly, the frequency of CD4 and CD8 T cells within the intratumoral T-cell population (CD8 NIVO $N = 20$; CD8 CTRL $N = 10$; CD4 NIVO $N = 20$; CD4 CTRL $N = 10$). **B,** Frequency of $CD8^+$ and $CD4^+$ T cells co-expressing the chemokine receptors CD183 (CXCR3) and CD195 (CCR5) in the tumor tissue of nivolumab-treated (NIVO) and control (CTRL) patients, for indication of CNS homing (CD8 NIVO $N = 12$; CD8 CTRL $N = 10$; CD4 NIVO $N = 14$; CD4 CTRL $N = 10$). **C** and **D,** The frequency of $CD4^+$ and $CD8^+$ T cells highly positive for CD183 (CD8 NIVO $N = 15$; CD8 CTRL $N = 10$; CD4 NIVO $N = 15$; CD4 CTRL $N = 10$) and CD195 (CD8 NIVO $N = 12$; CD8 CTRL $N = 10$; CD4 NIVO $N = 14$; CD4 CTRL $N = 10$), respectively, detected to compare the expression level of the chemokine receptors on intratumoral T cells in NIVO and control patients. **E,** Representative flow cytometry plot of Ab staining of tumor digest from NIVO and CTRL patients. Gating for T cells expressing high levels of chemokine receptors (CD183 and CD195) is marked with red. **F,** Frequency of $CD8^+$ T cells co-expressing CD183 and CD195 in blood samples from baseline (BL; surgical $N = 11$; nonsurgical $N = 14$), week (WK) 8 (surgical $N = 9$; nonsurgical $N = 11$), and WK16 (surgical $N = 5$; nonsurgical $N = 3$). Frequencies are compared between the surgical group and the tumor-bearing group (nonsurgical group). **G,** Frequency of T cells expressing Ki67 among intratumoral $CD8^+$ and $CD4^+$ T cells (CD8 NIVO $N = 13$; CD8 CTRL $N = 10$; CD4 NIVO $N = 14$; CD4 CTRL $N = 10$). **H,** Frequency of T cells expressing CD28 among intratumoral $CD8^+$ and $CD4^+$ T cells (CD8 NIVO $N = 14$; CD8 CTRL $N = 10$; CD4 NIVO $N = 15$; CD4 CTRL $N = 10$). **I,** Frequency of tissue-resident T cells expressing CD39 among intratumoral $CD8^+$ and $CD4^+$ T cells (CD8 NIVO $N = 14$; CD8 CTRL $N = 10$; CD4 NIVO $N = 15$; CD4 CTRL $N = 10$). **J,** Frequency of tissue-resident T cells expressing CD137 among intratumoral $CD8^+$ and $CD4^+$ T cells (CD8 NIVO $N = 14$; CD8 CTRL $N = 10$; CD4 NIVO $N = 15$; CD4 CTRL $N = 10$). For bar plots indicated, the mean and error bars show SD. Means were compared between NIVO and CTRL (tumor) and between the surgical group and the tumor-bearing group (nonsurgical group) at four time points (blood) using unpaired *t* test. *, $P < 0.05$; **, $P < 0.01$; ***, $P < 0.001$; ****, $P < 0.0001$. **K,** Volcano plot showing 1,716 differentially overexpressed genes and 260 underexpressed genes in NIVO patients ($N = 20$) compared with control patients ($N = 10$) based on bulk transcriptomic data. Overexpressed genes in NIVO are shown in red with an adjusted *P*-value < 0.05 and $\log_2$ fold change >2; underexpressed genes in NIVO patients are shown blue with adjusted *P*-value < 0.05 and $\log_2$ fold change <−2. The highlighted genes cover the most up- and downregulated genes and few immune-related genes of interest. Genes assed by flow cytometry are additionally marked.

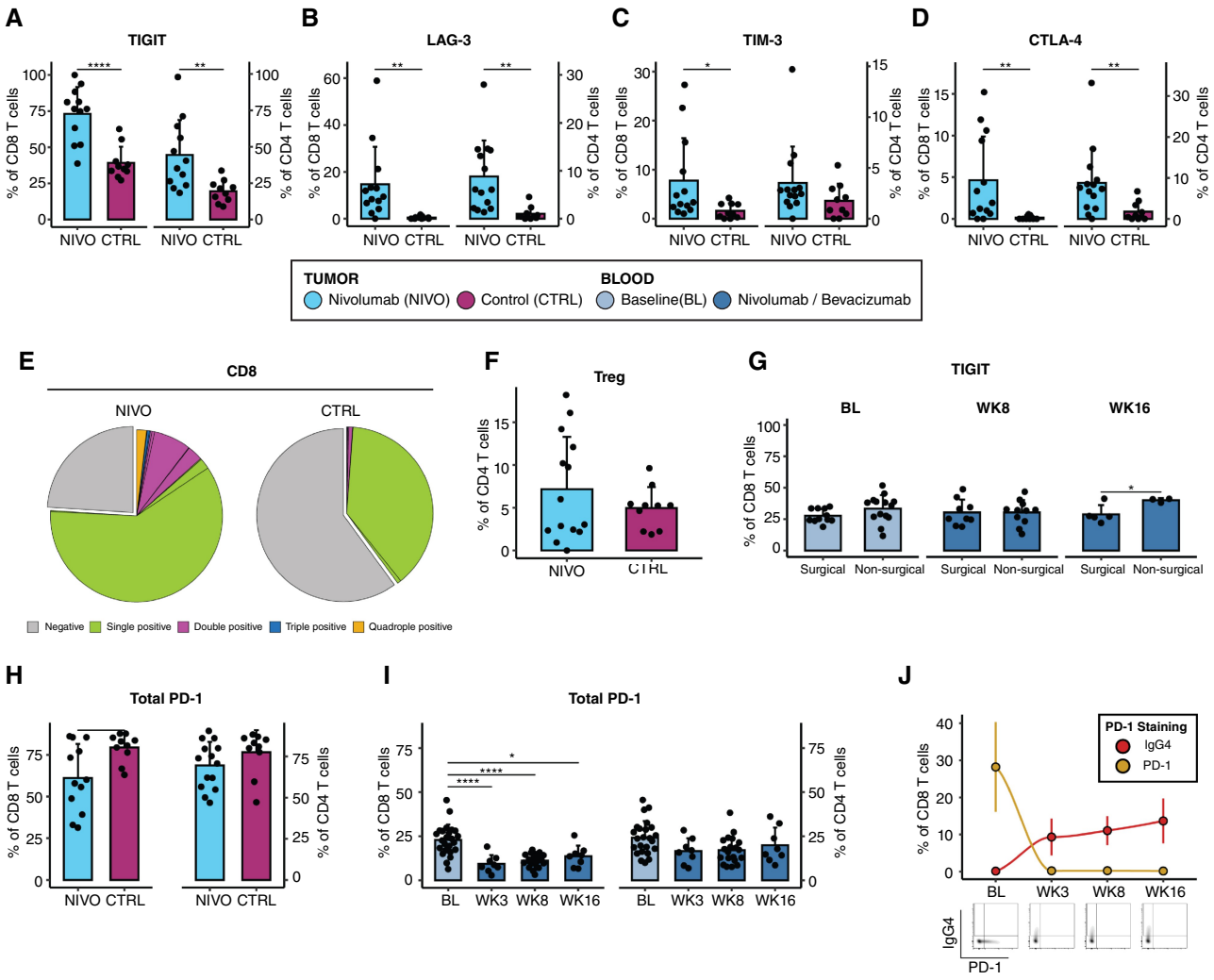

Figure 4.

Nivolumab induces late differentiation of T cells and an anti-inflammatory TME. **A–D,** Frequency of intratumoral CD8$^+$ T cells from NIVO and CTRL patients expressing inhibitory markers detected by flow cytometry: TIGIT (CD8 NIVO $N = 12$; CD8 CTRL $N = 10$; CD4 NIVO $N = 12$; CD4 CTRL $N = 10$; **A**), LAG-3 (**B**), TIM-3 (**C**), and CTLA-4 (CD8 NIVO $N = 13$; CD8 CTRL $N = 10$; CD4 NIVO $N = 14$; CD4 CTRL $N = 10$; **D**). **E,** Pie chart showing the proportion of intratumoral T cells expressing none or one or more of the studied inhibitory molecules (TIGIT, LAG-3, CTLA-4, TIM-3) within the nivolumab-treated patients (NIVO; $N = 12$) and the control patients (CTRL; $N = 10$). The pie charts are divided in negative cells (gray), single-positive (green), double-positive (purple), triple-positive (blue), and quadruple-positive cells (yellow). **F,** Frequency of Treg cells among intratumoral CD4$^+$ T cells from NIVO and CTRL patients (CD8 NIVO $N = 13$; CD8 CTRL $N = 10$; CD4 NIVO $N = 14$; CD4 CTRL $N = 10$). **G,** Frequency of CD8$^+$ T cells expressing TIGIT from blood samples at baseline (BL; surgical $N = 11$; nonsurgical $N = 14$), week (WK) 8 (surgical $N = 9$; nonsurgical $N = 11$), and WK16 (surgical $N = 5$; nonsurgical $N = 3$). Comparing the surgical group to the tumor-bearing group (nonsurgical) group. **H,** Frequency of the collected PD-1$^+$ population (based on anti-PD-1 and anti-IgG4 staining) within intratumoral T cells from nivolumab-treated (NIVO) and control (CTRL) patients (CD8 NIVO $N = 12$; CD8 CTRL $N = 10$; CD4 NIVO $N = 14$; CD4 CTRL $N = 10$). **I,** Frequency of a collected PD-1$^+$ population within PBMC-derived T cells collected at different time points of the treatment, before (BL; $N = 24$) and after (WK3 $N = 8$; WK8 $N = 20$; WK16 $N = 8$) nivolumab administration. **J,** Kinetics of nivolumab binding. CD8$^+$ T cells derived from blood collected before (BL; IgG4 $N = 23$; PD-1 $N = 39$) and after (WK3 IgG4 $N = 8$; PD-1 $N = 16$; WK8 IgG4 $N = 19$; PD-1 $N = 30$; WK16 IgG4 $N = 8$; PD-1 $N = 13$) nivolumab administration stained with anti-PD-1 (yellow) and anti-IgG4 (red); points represent mean, and error bars show SD. For bar plots indicated, the mean and error bars show SD. Means were compared between NIVO and CTRL (tumor), the surgical group, and the tumor-bearing group (nonsurgical group) at the four time points (blood) using unpaired *t* test. *, $P < 0.05$; **, $P < 0.01$; ***, $P < 0.001$; ****, $P < 0.0001$.

found in tumor tissue from NIVO patients compared with untreated control patients (**Fig. 4A–D**). Limited differences were observed in PBMCs for these markers before and after nivolumab administration (Supplementary Fig. S6), suggesting a tumor-specific effect. In addition, the frequencies of intratumoral CD8$^+$ and CD4$^+$ T cells expressing two or more of the inhibitory molecules, TIGIT, LAG-3, TIM-3, and CTLA-4, were significantly larger within the NIVO patients compared with the control patients (**Fig. 4E**; Supplementary Fig. S9). Specifically, the frequency of quadruple-positive CD8$^+$ T cells was significantly higher in NIVO patients, along with significantly higher frequencies of intratumoral T cells that were double positive for TIGIT and LAG-3 (CD4$^+$ and CD8$^+$)

and for TIGIT and TIM-3 ($CD8^+$; Supplementary Fig. S9). This suggests a major impairment of intratumoral T-cell function following nivolumab treatment. Finally, the level of regulatory T cells (Tregs) was low in tissue from controls but highly heterogeneous between NIVO patients (**Fig. 4F**), suggesting that also this T-cell subset may be altered.

The frequency of peripheral $CD8^+$ T cells expressing TIGIT in the nonsurgical group was found to be significantly higher at week 16 compared with the surgical group (**Fig. 4G**). This could indicate an ongoing exhaustion of T cells in the nonsurgical group, as the tumor was still present, and suggesting that chronic inflammation within the tumor tissue could be monitored by a peripheral upregulation of TIGIT.

Although upregulation of compensatory co-inhibitory molecules was observed, the level of PD-1 expression was decreased following nivolumab treatment. Intratumoral $CD8^+$ T cells expressing PD-1 were found in significantly lower frequencies in NIVO patients compared with control patients, and a similar trend was shown within intratumoral $CD4^+$ T cells (**Fig. 4H**). Furthermore, a significant drop in frequencies of peripheral PD-1-expressing $CD8^+$ T cells was observed after nivolumab treatment, and a similar trend was shown within peripheral $CD4^+$ T cells (**Fig. 4I**). PD-1 expression was measured using both anti-PD-1 and anti-IgG4 staining. The kinetics of nivolumab binding are shown in **Fig. 4J**, where PBMC-derived $CD8^+$ T cells were stained with anti-PD-1 and anti-IgG4. At baseline, PD-1 molecules on T cells were stained only by anti-PD-1, whereas after nivolumab administration, PD-1 molecules were instead stained by anti-IgG4. The sum of the T-cell populations stained by either anti-PD-1 or anti-IgG4 was therefore defined as the total PD-1^+ population (PD-1), to compare expression of PD-1 between time points and patient groups.

Thus, our data demonstrates that the T-cell activation signature observed following nivolumab treatment coincided with a profound upregulation of the checkpoint inhibition molecules TIGIT, LAG-3, TIM-3, and CTLA-4 on tumor-infiltrating T cells, whereas the expression of PD-1 declined after treatment initiation. The overall change in T-cell phenotypes following nivolumab treatment remained when excluding data from patients now classified as astrocytoma, IDH-mutant, WHO grade IV (Supplementary Fig. S10). Finally, no difference in these results was observed when removing patients receiving corticosteroid from analyses (Supplementary Fig. S11).

Tumor reactivity is detected in TILs from a fraction of patient with a distinct inflammatory profile

To further investigate the tumor recognition capacity of immune cells from nivolumab-treated patients, we tested the intracellular cytokine signature of expanded TILs when cocultured with autologous tumor digest. The reactivity of REP TILs against autologous tumor digest was demonstrated in four nivolumab-treated patients (NVB02, NVB05, NVB08, NVB10) out of 16 tested patients. REP TILs from patients NVB02 and NVB05 showed clear tumor recognition responses among both $CD4^+$ and $CD8^+$ T cells. For patient NVB10, we detected a small response only among $CD8^+$ T cells in REP TILs (**Fig. 5A**; Supplementary Figs. S12 and S13A). Overall tumor reactivity ranged between 1.2% and 13.6% of $CD8^+$ TILs and between 6.3% and 10.9% of $CD4^+$ TILs (**Fig. 5A**). To assess whether T-cell reactivity could influence patient outcome, we calculated the mOS and mPFS of the patients with reactive T cells to be 17.0 and 9.3 months, respectively. These were numerically higher compared with the NIVO patients without tumor-reactive TILs and mOS of 12.8 months and mPFS of 4.3 months (Supplementary Fig. S13B). However, the difference was not significant because of the small study cohort applicable to TIL reactivity analyses, and the results warrant further studies.

Transcriptomics analyses were performed to investigate differences in the TME between patients with tumor-reactive TILs and the rest of the surgical group within the nivolumab-treated patients. The DEA showed 1,522 differentially expressed genes, and large differences in the TME were observed, revealing a cluster-split dividing patients with tumor-reactive versus tumor nonreactive TILs (**Fig. 5B**). The overexpressed genes observed in the patients with reactive TILs included *TGFB1*, *CXCL13*, and *IL31RA*, which are all related to inflammation (**Fig. 5B**). In addition, from a GSEA, we identified differential overexpression of the MHC class I (MHC-I) peptide presentation pathway in patients with tumor-reactive TILs (**Fig. 5C**), which was supported by higher HLA class I expression among tumor digest-derived live cells from patients with tumor-reactive TILs (Supplementary Fig. S14). The cluster-split dividing patients with tumor-reactive versus tumor nonreactive TILs was additionally confirmed in a proteomics analysis (Supplementary Fig. S15). Additionally, when assessing the T-cell characteristics, we observed a tendency for higher frequencies of T cells expressing CD28 as well as T cells expressing the inhibitory receptor TIGIT in tumors from patients with reactive TILs compared with the remaining NIVO patients (Supplementary Fig. S13C). Furthermore, a significantly higher frequency of Tregs among $CD4^+$ T cells was detected in patients with tumor-reactive TILs (Supplementary Fig. S13C). In summary, the TME of the patients with tumor-reactive TILS had a different gene expression profile than the remaining NIVO patients and an expression suggesting stronger T-cell activation and antigen presentation yet counterbalanced by inhibitory TIGIT expression and Treg presence.

Tumor-specific NARTs are present in tumor and periphery of GBM patients

There has been limited exploration of the antigen landscape of relevance for T-cell recognition of GBM. Therefore, we aimed to determine if tumor recognition could be driven by tumor mutation-derived neoepitopes. To determine if neoepitopes could be targets for tumor cell recognition by T cells in patients with tumor-reactive TILs, we screened for the presence of NARTs in both TILs and PBMCs, during treatment. Neoepitopes were predicted from the WES and RNA sequencing from the primary and recurrent tumors. We screened PBMCs, YTILs, and REP TILs for $CD8^+$ T-cell recognition of neoepitopes using this personalized library of predicted neoepitopes and a pool of virus-derived epitopes, selected based on the patients' HLA profile, to determine the level of virus antigen-reactive $CD8^+$ T cells as a comparator. The screening was conducted using fluorescent and DNA barcode-labelled pMHC multimers, allowing pooling of 134 to 183 neoepitope pMHC multimers (PE labeled) and 3 to 16 virus-derived pMHC multimers (APC labeled) per sample (**Fig. 6A**). We identified NART populations against 2 to 6 neoepitope/MHC per patient in PBMCs and/or TILs (**Fig. 6B**; Supplementary Fig. S16). This level of recognition was comparable to other cohorts of patients, with urothelial carcinoma and melanoma previously evaluated for NARTs (49, 50), despite the overall lower tumor mutational burden in GBM tumors. The total numbers of responses across all evaluated patients are shown in **Fig. 6C**, and the sum of estimated frequencies of NARTs and virus antigen-reactive $CD8^+$ T cells is shown in **Fig. 6D**, both for each blood sample and for the TILs. When studying the dynamics of NARTs, there was an

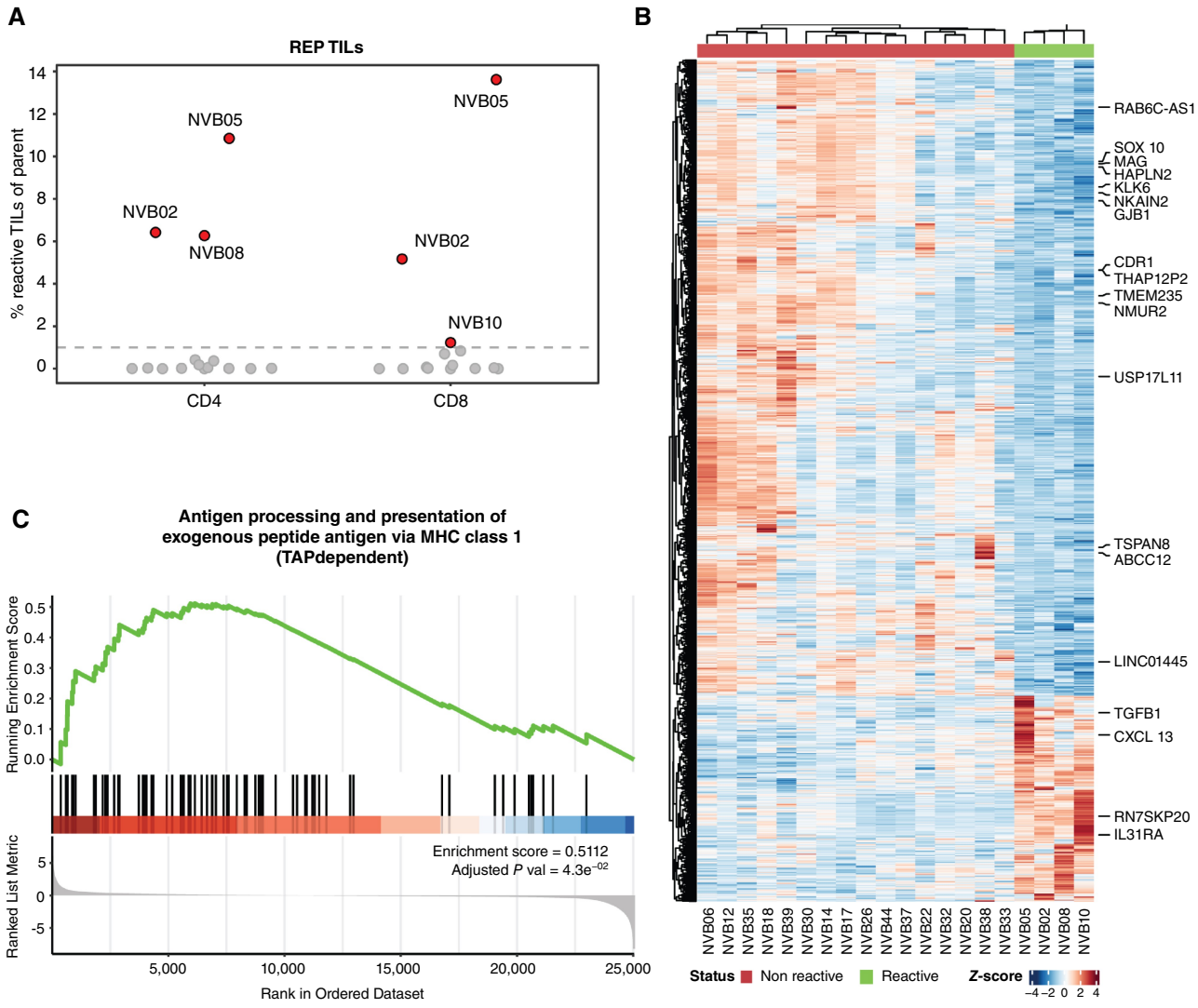

Figure 5.

Comparison of patients with reactive T cells vs. nonreactive T cells. **A,** Reactivity toward autologous tumor digest detected in CD8 ($N = 14$) and CD4 ($N = 15$) REP TILs. TILs were cocultured with autologous tumor digest for 8 hours and hereafter intracellularly stained for TFN-α, IFN-γ, and CD137 and surface stained for CD107a. TILs expressing at least two of the markers were defined as reactive. Background reactivity (TILs alone) is subtracted, and hereafter patients with more than 1% reactive TILs are defined as reactive. Patients with tumor-reactive TILs are highlighted in red. Patients without tumor-reactive TILs are marked in gray. **B,** 372 differential overexpressed and 1,150 differentially underexpressed genes were found in patients with reactive T cells by differential expression analysis with an adjusted *P*-value < 0.05. These differentially expressed genes are illustrated by a heatmap showing that patients with reactive ($N = 4$) and nonreactive ($N = 16$) T cells were defining the two first unsupervised clusters. The highlighted genes consist of the most up- and downregulated genes and include some immune-related genes of interest. **C,** A gene set enrichment analysis was made from the DEA, and "antigen presentation on MHC-I" was found as an enriched pathway for patients with reactive T cells.

increased breadth of neoepitope recognition after nivolumab treatment (week 3) in patients NVB02 and NVB05, which thereafter persisted. The same pattern was observed for the magnitude of the T-cell responses (i.e., the sum of estimated frequencies) at weeks 3 and 8, especially for NVB02. NART responses were only found at baseline and at week 8 in PBMCs from NVB10. However, the breadth and magnitude appeared to increase at week 8. Neoepitope responses were only detected in TILs from NVB02 and NVB05, where both the breadth and magnitude increased in REP TILs compared with YTILs, most dominant in TILs from NVB02. The number of responses toward virus peptides in PBMCs remained consistent throughout the treatment period, as did the magnitude of these. All T-cell responses were confirmed by a 14-day patient-specific peptide stimulation of PBMCs (Supplementary Fig. S17).

In summary, we screened for NARTs in YTILs, REP TILs, and PBMCs. We found NARTs in TILs from NBV02 and NVB05. Even though the sum of estimated frequencies of detected NART was low in these patients, it coincided with NVB02 and NVB05 having the highest frequencies of reactive $CD8^+$ TILs upon tumor challenge, whereas NVB10 had relatively few tumor-reactive $CD8^+$ TILs, and NVB08 had no tumor-reactive $CD8^+$ TILs (**Fig. 5A**). Thus, tumor mutation-derived neoepitopes do appear to constitute a fraction of

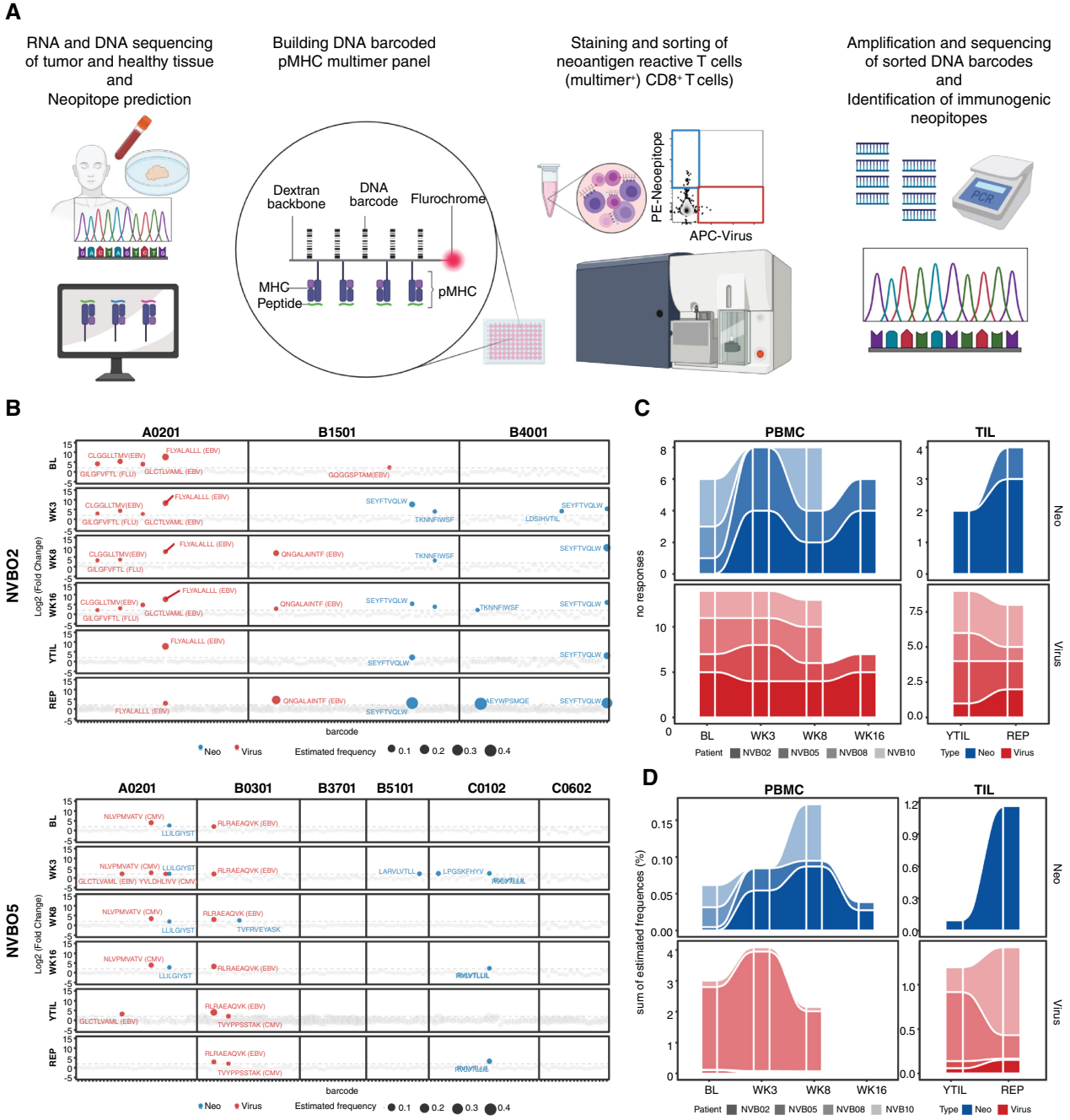

Figure 6.

Detection of neoantigen-reactive CD8$^+$ T cells (NART). **A,** Illustrative explanation of NART detection. Neoantigens were predicted based on whole-exome sequencing (WES) and RNA sequencing of tumor and WES of healthy tissue (blood). A patient-specific panel of DNA-barcoded pMHC multimers was assembled with the predicted neopeptides and virus peptides. Patient material (TILs and PBMCs) was stained with a pool of the multimer panel, and multimer$^+$ CD8$^+$ T cells were sorted based on their fluorochrome label: PE (blue) for neopeptides and APC (red) for virus peptides. The DNA barcodes bound to the sorted T cells were hereafter amplified by PCR and sequenced. Enriched and hereby immunogenic neopeptide–MHC and virus peptide–MHC complexes were identified based on the corresponding DNA barcode. **B,** Screening output for patient NVB02 and NVB05. Significantly enriched ($P < 0.001$; $\log_2$ fold change >2) barcoded pMHC multimers are colored and labelled with the immunogenic peptide sequence. Virus antigens are marked in red, and neoantigens are marked in blue. The dot size represents an estimated frequency of CD8$^+$ T cells for each neoantigen-reactive CD8$^+$ T cell (NART). Gray dots are all pMHC multimers that where not significantly enriched after sample staining. Specificities are shown for each blood sample time point: baseline (BL), week (WK) 3, WK8, WK16, and for both young TILs (YTIL) and rapidly expanded (REP) TILs. The screened pMHCs are additionally divided based on HLA type. **C,** Number of responses toward different neoantigens (blue) and virus antigens (red). Individual patients are marked in different shades of respective colors. The plot is further divided in PBMC and TILs. There was no significant difference between blood sample time points or between YTILs and REP TILs. **D,** Sum of estimated frequency of NARTs shown in percentage out of all CD8$^+$ T cells recognizing different neoantigens (blue) and virus antigens (red). There was also no significant difference between blood sample time points or between YTILs and REP TILs.

the tumor-reactive response, and such T-cell responses were also detected in the periphery.

We further observed that the patients with tumor-reactive $CD8^+$ TILs (NVB02, NVB05, NVB10) were those with the highest proportional overlap of mutations when comparing primary and recurrent tumor (Supplementary Fig. S18A), suggesting that such recognition may be dominated by clonal neoantigen recognition. In addition, we observed three neoepitopes recognized by NARTs in patient NVB05 (LLILGIYST-A0201, LARVLVTLL-B5101, RVLVTLLIL-C0102), which originated from the same frameshift mutation from the gene, *NF1* (Supplementary Fig. S18B), suggesting extraordinary immunogenicity of this genetic alteration, which opens a possibility to explore this further as a potential shared neoantigen source.

Discussion

We report data from a translational phase 2 clinical study where we treated patients with recurrent GBM with nivolumab and bevacizumab every 2 weeks until progression, death, or intolerable toxicity. We showed that it was feasible and safe to use nivolumab and bevacizumab in this setting, but we could not demonstrate any direct benefit of nivolumab combined with bevacizumab on PFS or OS, when compared with historical control or when compared with control patients included in the immune analyses. The small cohort size could potentially mask survival benefits from the given treatment, as Cloughesy and colleagues have previously shown that neoadjuvant anti-PD-1 therapy extended survival compared with adjuvant anti-PD-1 therapy (51). We did observe a few patients who unexpectedly, based on existing clinical parameters, became long-term survivors, which could indicate therapeutic benefit in a subset of patients. Moreover, this study additionally offered a unique opportunity to explore the immune infiltration to GBM tumors and the potential impact of nivolumab treatment on the immune landscape.

Researchers are still in the early stages of understanding the immune system of the brain, and little is known about the peripheral immune cells' role in the brain. We examined intratumoral T cells in patients with recurrent GBM, by evaluating the cellular impact of nivolumab treatment. Moreover, we studied the effect of nivolumab and bevacizumab treatment on peripheral T cells in patients who did (surgical group) and did not (nonsurgical group) receive resection of their recurrent tumor.

Importantly, we were able to detect nivolumab in brain tumors only 7 days after administration to the patient, documenting the capacity for such antibodies to penetrate to this challenging location. However, it can be questioned whether nivolumab entered as free molecules or bound to T cells. The BBB strongly regulates passage of large molecules and cells into the brain tissue through tight junction (13), but it has also been shown that the BBB in GBM can be disrupted and become more permeable in these tight junctions, which supports both scenarios (14, 15). We found that PD-1 molecules on all intratumoral T cells were saturated by nivolumab in unrested tumor digest; this also included tissue-resident T cells within tumor tissue. This implies that nivolumab can penetrate the tumor as free immunoglobulins. Previously, Osa and colleagues showed that, when nivolumab-pretreated T cells were cultured in nivolumab-free medium for more than 24 hours, the nivolumab bound to the T cells where lost. Moreover, they also showed that decreased concentrations of nivolumab in plasma correlated with a drop in the level of nivolumab-bound T cells in blood from patients with non-small cell lung cancer (52). Considering the findings of Osa and colleagues, our results indicate that nivolumab has been in excess in the TME as intratumoral T cells were saturated by nivolumab, which further support the notion that nivolumab can enter the GBM microenvironment as an immunoglobulin alone.

We found that nivolumab treatment affected T-cell phenotypic characteristics, both in the tumor and in the periphery, and moreover we could observe an effect on the TME based on RNA sequencing of tumor tissue. Intratumoral T cells exhibited elevated CD183 and CD195 chemokine receptor expression following nivolumab administration. Previous studies have shown CD195 and CD183 T-cell co-expression in CSF and PBMCs of patients with neurological inflammation, distinguishing them from non-inflammatory neurological diseases (46, 47). Our findings suggest that nivolumab treatment induces increased neuroinflammation, potentially enhancing recruitment to the GBM tumor. Additionally, nivolumab/bevacizumab-treated patients who retained their tumor showed higher frequencies of $CD8^+$ T cells expressing CD183 and CD195 in the blood compared with patients who underwent tumor resection. This observation supports the idea of active recruitment of peripheral T cells to the brain because of neurological inflammation, even in the context of cancer. However, further investigation is warranted to assess the presence of CNS homing T cells in both blood and CSF in the two patient groups. Furthermore, in nivolumab-treated patients, intratumoral T cells demonstrated increased activation signatures and expression of CD39 and CD137 compared with control patients, which potentially indicates an enrichment of tumor-reactive T cells. CD39, when co-expressed with CD103, has previously been associated with extended survival in patients with head and neck cancer (53). We observed that $CD39^+$ tissue-resident $CD8^+$ T cells were more prevalent in tumor digest from nivolumab-treated patients compared with control patients. Increased frequencies of CD39 expressing T cells can furthermore indicate an increased tumor-specific T-cell activation, as CD39 has previously been suggested as a marker to differentiate tumor-specific T cells from bystander T cells within the TME (54). Although CD39 is expressed late and upon T-cell activation, CD137 expression both increases and attenuates quickly after T-cell antigen recognition and stimulation (55–59). We found a trend for increased expression of CD137 on tissue-resident $CD8^+$ T cells after nivolumab treatment. Such cells were present at low frequencies, which could be explained by the transient expression kinetics of CD137 expression (56). Collectively, PD-1-blockade likely resulted in increased TCR activation of intratumoral T cells, also supported by overexpression of *FGFBP2*, a gene linked to T-cell cytotoxicity (60, 61). Moreover, the co-stimulatory molecule CD28 was expressed on intratumoral T cells with varying frequencies among $CD8^+$ T cells within nivolumab-exposed tumors. Previous studies have shown that $CD28^+$ T cells respond well to anti-PD-1 therapy and that loss of CD28 on $CD8^+$ T cells is a marker for unresponsive patients (62, 63). We observed that a high frequency of intratumoral $CD28^+CD8^+$ T cells correlated with longer PFS and OS after recurrence only in nivolumab-treated patients, suggesting CD28 to be a marker of favorable T-cell response also in GBM. PD-1 acts primarily by inhibiting the co-stimulatory signal through CD28, rather than TCR signaling (64). It is possible that nivolumab not only blocks the inhibitory signaling through PD-1 but also enables T cells to upregulate CD28 expression and thus facilitates co-stimulation. This co-stimulation and activation may lead to expansion and proliferation of tumor-specific T-cell clones, a notion supported by the higher frequency of $Ki67^+$ intratumoral T cells we observed within nivolumab-treated patients. Previous studies have shown that

TILs in GBM exhibit a highly exhausted phenotype, primarily reflected in the high expression of PD-1 (65, 66), but despite the enhanced intratumoral T-cell activation and proliferation following nivolumab treatment, an anti-inflammatory TME also appeared to be augmented, perhaps as a feedback mechanism in response to an increased immune activation caused by PD-1 blockade. Upregulation of several other inhibitory molecules, e.g., LAG-3, TIM-3, CTLA-3, and TIGIT, was found to occur on intratumoral T cells following nivolumab treatment, thus contributing to drug resistance (67). In particular, TIGIT was expressed on a larger fraction of T cells and could serve as a relevant co-target as has previously been suggested (68, 69). We observed that the frequency of PD-1^{+}CD8^{+} T cells decreased following nivolumab treatment both in tumor and in the periphery. This could be because of endocytosis of the receptor after nivolumab binding, as the case is for other receptors after engagement of their target (70, 71), but it needs to be evaluated further. Upregulation of additional inhibitory receptors could be a compensatory mechanism upon PD-1 downregulation. Overall, our T-cell phenotypic findings are consistent with recent research by Lee and colleagues, who observed heightened T-cell infiltration, elevated expression of neuroinflammation-associated chemokines (XCL1, XCL2, and CCL5), and upregulation of genes related to T-cell activation and exhaustion, including TIGIT, in response to neoadjuvant anti-PD-1 treatment (72). Collectively, this indicates a positive effect of neoadjuvant therapy within this tumor type. Moreover, our study demonstrates T-cell activation and TME modulation occurring within a considerably short period of only 7 days from nivolumab administration to tumor resection, whereas other neoadjuvant anti-PD-1 clinical studies show the effect 14 days after administration (51, 72–74). However, it becomes evident that combinatorial therapy is necessary to effectively counteract inhibitory and anti-inflammatory mechanisms induced upon anti-PD-1 treatment.

Beyond T-cell phenotyping, we were able to detect tumor reactivity in REP TILs from 25% (4 out of 16) of nivolumab-treated patients. We found a clear difference in the TME landscape of patients with tumor-reactive TILs compared with the remaining nivolumab-treated patients based on transcriptomic data. Specifically, we found gene set enrichment of an immune-related pathway involved in antigen processing and presentation of MHC-I. This could indicate an active immune reaction with INFγ release, which is known to induce HLA expression (75), resulting in an ongoing presentation of potential immunogenic neoepitopes to T cells within the TME of these patients, providing a potential for CD8^{+} T cell-mediated cancer cell killing (76, 77). We therefore examined the tumor specificity of the reactive TILs further by screening PBMCs and TILs for the presence of NARTs. We were able to detect NARTs in TILs from two patients, which corresponded to patients who showed the highest reactivity against tumor. NARTs detected in these patients (NVB02 and NVB05) were specific to neoantigens found in both the primary and recurrent tumors, potentially representing clonal mutations. In fact, we detected three immunogenic neoepitopes from patient NVB05 derived from a frameshift mutation in *NF1*. Mutations in the *NF1* gene have been reported in 13% to 14% of GBM, hereof 78% consisting of frameshifts (78). Additionally, *NF1* mutations have been described to be related to high T-cell infiltration in gliomas (79). Therefore, such mutations could be of interest as potential biomarkers for use in immunotherapy treatment. Consistent with this, the T-cell infiltration and quality of neoantigens, and thereby the potential to induce a potent tumor-specific T-cell response, have previously been correlated with longer survival for GBM patients (80). Our results support this with a higher PFS and OS after recurrence for patients with tumor-reactive TILs, compared with the remaining patients in the nivolumab-treated group, though it was not significant in this small patient group. Personalized neoantigen vaccines have been tested to induce and boost the NART repertoire in patients with GBM, but despite tumor infiltration of vaccine-induced NARTs, immune suppressive factors diminished the immune response (81, 82).

Finally, an increasing number of observations suggest that the peripheral immune system plays a role in the immunosurveillance of the brain (6–9). We detected the same NART populations in both blood and tumor samples, confirming an interaction between the brain tumor and the peripheral immune system. This is consistent with a study identifying GBM-specific NARTs in blood (83), whereas Lee and colleagues showed an overlap in TCR repertoire in activated/exhausted T cells within PBMCs and TILs (72). Moreover, we found that both the number and the sum of estimated frequency of the NARTs increased after nivolumab treatment. This aligns with previous observations from other cancer cohorts, where therapy targeting the PD-1/PD-L1 axis resulted in a boost of the number of NARTs in PBMC shortly after treatment initiation (49).

In conclusion, we report that nivolumab can penetrate GBM tumors, likely as a free molecule. Within a timeframe of only 7 days, nivolumab induced notable changes in intratumoral T-cell phenotypes and in the gene expression profile of the TME. Additionally, we identified neoantigen-reactive CD8^{+} T cells in tumor-reactive TILs and in PBMC, and these NARTs appeared to be boosted after nivolumab administration. Altogether, our data, together with other neoadjuvant studies, suggest that to improve immunotherapies for GBM, it is of foremost important to consider the complexity of the tumor and the resistance mechanism(s) induced after PD-1.

Authors' Disclosures

S.K. Skadborg reports grants from the Danish Cancer Society, Læge Sofus Carl Emil Friis og Hustru Olga Doris Friis' Legat, and the Novo Nordisk Research Foundation during the conduct of the study. S. Maarup reports grants from the Danish Cancer Society and grants from Læge Sofus Carl Emil Friis og Hustru Olga Doris Friis' Legat outside the submitted work. A. Draghi reports personal fees from AstraZeneca outside the submitted work. H.S. Poulsen reports grants from the Danish Cancer Society and Læge Sofus Carl Emil Friis og Hustru Olga Doris Friis' Legat during the conduct of the study. B. Hasselbalch reports grants from the Danish Cancer Society and Læge Sofus Carl Emil Friis og Hustru Olga Doris Friis' Legat during the conduct of the study. I.M. Svane reports grants from Evaxion Biotech, Adaptimmune, IO Biotech, Lytix Biopharma, TILT Biotherapeutics, Enara Bio, and Asgard Biotech; reports personal fees from MSD, IO Biotech, Novartis, Pierre Fabre, TILT Biotherapeutics, Sanofi Aventis, BMS, Novo Nordisk, and Takeda outside the submitted work; and has a stock in IO Biotech—personally received relatlimab for clinical trial from BMS. U. Lassen reports personal fees from Bayer and Novartis and grants from Roche, GSK, Incyte, Lilly, and Janssen during the conduct of the study. S.R. Hadrup reports grants from Læge Sofus Carl Emil Friis og Hustru Olga Doris Friis' Legat, the Novo Nordisk Research Foundation, and the Danish Cancer Society during the conduct of the study and nonfinancial support from PokeAcell and TetramerShop outside the submitted work; in addition, S.R. Hadrup has a patent for WO2015188839 licensed to Immudex and a patent for WO2020064915 licensed to 10x Genomics. No disclosures were reported by the other authors.

Authors' Contributions

S.K. Skadborg: Data curation, formal analysis, investigation, visualization, methodology, writing–original draft, project administration, writing–review and editing. **S. Maarup:** Data curation, formal analysis, investigation, visualization, methodology, writing–original draft, project administration, writing–review and editing. **A. Draghi:** Data curation, formal analysis, writing–review and editing. **A. Borch:** Data curation, formal analysis, visualization, writing–review and editing. **S.**

Hendriksen: Data curation, writing–review and editing. **F. Mundt:** Data curation, writing–review and editing. **V. Pedersen:** Data curation, visualization, writing–review and editing. **M. Mann:** Data curation, supervision, writing–review and editing. **I.J. Christensen:** Data curation, visualization, writing–review and editing. **J. Skjøth-Rasmussen:** Supervision, Writing–review and editing. **C.W. Yde:** Data curation, writing–review and editing. **B.W. Kristensen:** Data curation, supervision, funding acquisition, writing–review and editing. **H.S. Poulsen:** Conceptualization, supervision, funding acquisition, writing–review and editing. **B. Hasselbalch:** Conceptualization, supervision, funding acquisition, writing–review and editing. **I.M. Svane:** Conceptualization, supervision, funding acquisition, writing–review and editing. **U. Lassen:** Conceptualization, data curation, supervision, funding acquisition, investigation, writing–review and editing. **S.R. Hadrup:** Conceptualization, resources, supervision, funding acquisition, investigation, visualization, methodology, writing–original draft, project administration, writing–review and editing.

Acknowledgments

We thank all patients who donated material that was used in this study, the funding that supported this research, Group leader, MD, PhD M. Donia and M. Presti for invaluable support and critical review of the manuscript and assistant with laboratory work, PhD T. Tamhane and A.D. Burkal for the production of MHC class I monomers, B. Rotbøl and A.F. Løye for technical assistance handling the flow cytometry instruments and samples, and O. S. G. Heiede for technical assistance with flow cytometry analysis. The work was funded by the Danish Cancer Society (R204-A12416), Læge Sofus Carl Emil Friis og Hustru Olga Doris Friis' Legat, and the Novo Nordisk Research Foundation [Challenge Grant NNF21OC0066562, Center for Nano Immune Cell Engineering (NICE)], and Bristol Myers Squibb generously provided nivolumab.

Note

Supplementary data for this article are available at Cancer Immunology Research Online (http://cancerimmunolres.aacrjournals.org/).

Received November 14, 2023; revised March 10, 2024; accepted June 14, 2024; published first June 17, 2024.

References

1. Stupp R, Mason WP, van den Bent MJ, Weller M, Fisher B, Taphoorn MJB, et al. Radiotherapy plus concomitant and adjuvant temozolomide for glioblastoma. N Engl J Med 2005;352:987–96.
2. Wen PY, Weller M, Lee EQ, Alexander BM, Barnholtz-Sloan JS, Barthel FP, et al. Glioblastoma in adults: a Society for Neuro-Oncology (SNO) and European Society of Neuro-Oncology (EANO) consensus review on current management and future directions. Neuro Oncol 2020;22:1073–113.
3. Schalper KA, Rodriguez-Ruiz ME, Diez-Valle R, López-Janeiro A, Porciuncula A, Idoate MA, et al. Neoadjuvant nivolumab modifies the tumor immune microenvironment in resectable glioblastoma. Nat Med 2019;25:470–6.
4. Arrieta VA, Chen AX, Kane JR, Kang SJ, Kassab C, Dmello C, et al. ERK1/2 phosphorylation predicts survival following anti-PD-1 immunotherapy in recurrent glioblastoma. Nat Cancer 2021;2:1372–86.
5. Medawar PB. Immunity to homologous grafted skin; the fate of skin homografts transplanted to the brain, to subcutaneous tissue, and to the anterior chamber of the eye. Br J Exp Pathol 1948;29:58–69.
6. Bartholomäus I, Kawakami N, Odoardi F, Schläger C, Miljkovic D, Ellwart JW, et al. Effector T cell interactions with meningeal vascular structures in nascent autoimmune CNS lesions. Nature 2009;462:94–8.
7. Louveau A, Smirnov I, Keyes TJ, Eccles JD, Rouhani SJ, Peske JD, et al. Structural and functional features of central nervous system lymphatic vessels. Nature 2015;523:337–41.
8. Aspelund A, Antila S, Proulx ST, Karlsen TV, Karaman S, Detmar M, et al. A dural lymphatic vascular system that drains brain interstitial fluid and macromolecules. J Exp Med 2015;212:991–9.
9. das Neves SP, Delivanoglou N, Da Mesquita S. CNS-draining meningeal lymphatic vasculature: roles, conundrums and future challenges. Front Pharmacol 2021;12:655052.
10. Nayak L, Molinaro AM, Peters K, Clarke JL, Jordan JT, de Groot J, et al. Randomized phase II and biomarker study of pembrolizumab plus bevacizumab versus pembrolizumab alone for patients with recurrent glioblastoma. Clin Cancer Res 2021;27:1048–57.
11. Reardon DA, Kim TM, Frenel JS, Simonelli M, Lopez J, Subramaniam DS, et al. Treatment with pembrolizumab in programmed death ligand 1–positive recurrent glioblastoma: results from the multicohort phase 1 KEYNOTE-028 trial. Cancer 2021;127:1620–9.
12. Larkin J, Chiarion-Sileni V, Gonzalez R, Grob J-J, Rutkowski P, Lao CD, et al. Five-year survival with combined nivolumab and ipilimumab in advanced melanoma. N Engl J Med 2019;381:1535–46.
13. Pluim D, Ros W, van Bussel MTJ, Brandsma D, Beijnen JH, Schellens JHM. Enzyme linked immunosorbent assay for the quantification of nivolumab and pembrolizumab in human serum and cerebrospinal fluid. J Pharm Biomed Anal 2019 Feb 5;164:128–34.
14. Liebner S, Fischmann A, Rascher G, Duffner F, Grote EH, Kalbacher H, et al. Claudin-1 and claudin-5 expression and tight junction morphology are altered in blood vessels of human glioblastoma multiforme. Acta Neuropathol 2000;100:323–31.
15. Wolburg H, Wolburg-Buchholz K, Kraus J, Rascher-Eggstein G, Liebner S, Hamm S, et al. Localization of claudin-3 in tight junctions of the blood-brain barrier is selectively lost during experimental autoimmune encephalomyelitis and human glioblastoma multiforme. Acta Neuropathol 2003;105:586–92.
16. Pointer KB, Clark PA, Schroeder AB, Salamat MS, Eliceiri KW, Kuo JS. Association of collagen architecture with glioblastoma patient survival. J Neurosurg 2017;126:1812–21.
17. Reardon DA, Gokhale PC, Klein SR, Ligon KL, Rodig SJ, Ramkissoon SH, et al. Glioblastoma eradication following immune checkpoint blockade in an orthotopic, immunocompetent model. Cancer Immunol Res 2016;4:124–35.
18. Park J, Kim CG, Shim JK, Kim JH, Lee H, Lee JE, et al. Effect of combined anti-PD-1 and temozolomide therapy in glioblastoma. Oncoimmunology 2018;8:e1525243.
19. Reardon DA, Brandes AA, Omuro A, Mulholland P, Lim M, Wick A, et al. Effect of nivolumab vs bevacizumab in patients with recurrent glioblastoma: the CheckMate 143 phase 3 randomized clinical trial. JAMA Oncol 2020;6:1003–10.
20. Donia M, Junker N, Ellebaek E, Andersen MH, Straten PT, Svane IM. Characterization and comparison of "standard" and "young" tumour-infiltrating lymphocytes for adoptive cell therapy at a Danish Translational Research Institution. Scand J Immunol 2012;75:157–67.
21. Andersen R, Borch TH, Draghi A, Gokuldass A, Rana MAH, Pedersen M, et al. T cells isolated from patients with checkpoint inhibitor-resistant melanoma are functional and can mediate tumor regression. Ann Oncol 2018;29:1575–81.
22. Draghi A, Chamberlain CA, Khan S, Papp K, Lauss M, Soraggi S, et al. Rapid identification of the tumor-specific reactive TIL repertoire via combined detection of CD137, TNF, and IFNγ, following recognition of autologous tumor-antigens. Front Immunol 2021;12:4236.
23. Abrahimi P, Chang WG, Kluger MS, Qyang Y, Tellides G, Saltzman WM, et al. Efficient gene disruption in cultured primary human endothelial cells by CRISPR/Cas9. Circ Res 2015;117:121–8.
24. Krueger F. Trim Galore [Internet]. 2019 [cited 2022 Feb 7]. Available from: https://github.com/FelixKrueger/TrimGalore.
25. Martin M. Cutadapt removes adapter sequences from high-throughput sequencing reads. EMBnet.journal 2011;17:10.
26. Andrews S. FastQC [Internet]. 2019 [cited 2022 Feb 7]. Available from: https://www.bioinformatics.babraham.ac.uk/projects/fastqc.
27. Lab P. Kallisto [Internet]. 2019 [cited 2022 Feb 9]. Available from: https://pachterlab.github.io/kallisto/.
28. Genome Reference Consortium. Genome reference consortium human build 38 patch release 14 (GRCh38.p14) [Internet]. 2022 [cited 2022 Jul 4]. Available from: https://www.ncbi.nlm.nih.gov/assembly/GCF_000001405.40.
29. Geyer PE, Kulak NA, Pichler G, Holdt LM, Teupser D, Mann M. Plasma proteome profiling to assess human health and disease. Cell Syst 2016;2:185–95.
30. Meier F, Brunner AD, Frank M, Ha A, Bludau I, Voytik E, et al. diaPASEF: parallel accumulation–serial fragmentation combined with data-independent acquisition. Nat Methods 2020;17:1229–36.

31. Love MI, Huber W, Anders S. Moderated estimation of fold change and dispersion for RNA-seq data with DESeq2. Genome Biol 2014;15:550.
32. Wu T, Hu E, Xu S, Chen M, Guo P, Dai Z, et al. clusterProfiler 4.0: a universal enrichment tool for interpreting omics data. Innovation (Camb) 2021;2: 100141.
33. Gu Z, Eils R, Schlesner M. Complex heatmaps reveal patterns and correlations in multidimensional genomic data. Bioinformatics 2016;32:2847–9.
34. Yu G. Visualization of functional enrichment result. R package version 1.10.2. Mol Ther Nucleic Acids 2021. https://rdrr.io/bioc/enrichplot/.
35. McKenna A, Hanna M, Banks E, Sivachenko A, Cibulskis K, Kernytsky A, et al. The genome analysis toolkit: a MapReduce framework for analyzing next-generation DNA sequencing data. Genome Res 2010;20: 1297–303.
36. Li H. Aligning sequence reads, clone sequences and assembly contigs with BWA-MEM. arXiv 2013;1–3. https://doi.org/10.48550/arXiv.1303.3997.
37. Cibulskis K, Lawrence MS, Carter SL, Sivachenko A, Jaffe D, Sougnez C, et al. Sensitive detection of somatic point mutations in impure and heterogeneous cancer samples. Nat Biotechnol 2013;31:213–19.
38. Bjerregaard AM, Nielsen M, Hadrup SR, Szallasi Z, Eklund AC. MuPeXI: prediction of neo-epitopes from tumor sequencing data. Cancer Immunol Immunother 2017;66:1123–30.
39. Reynisson B, Alvarez B, Paul S, Peters B, Nielsen M. NetMHCpan-4.1 and NetMHCIIpan-4.0: improved predictions of MHC antigen presentation by concurrent motif deconvolution and integration of MS MHC eluted ligand data. Nucleic Acids Res 2020;48:W449–54.
40. Weese D, Holtgrewe M, Reinert K. RazerS 3: faster, fully sensitive read mapping. Bioinformatics 2012;28:2592–9.
41. Szolek A, Schubert B, Mohr C, Sturm M, Feldhahn M, Kohlbacher O. OptiType: precision HLA typing from next-generation sequencing data. Bioinformatics 2014;30:3310–16.
42. Bentzen AK, Marquard AM, Lyngaa R, Saini SK, Ramskov S, Donia M, et al. Large-scale detection of antigen-specific T cells using peptide-MHC-I multimers labeled with DNA barcodes. Nat Biotechnol 2016;34:1037–45.
43. Louis DN, Perry A, Wesseling P, Brat DJ, Cree IA, Figarella-Branger D, et al. The 2021 WHO classification of tumors of the central nervous system: a summary. Neuro Oncol 2021;23:1231–51.
44. Basch E, Schrag D. The evolving uses of "Real-World" data. JAMA 2019;321: 1359–60.
45. Urup T, Dahlrot RH, Grunnet K, Christensen IJ, Michaelsen SR, Toft A, et al. Development and validation of a prognostic model for recurrent glioblastoma patients treated with bevacizumab and irinotecan. Acta Oncol 2016;55:418–22.
46. Giunti D, Borsellino G, Benelli R, Marchese M, Capello E, Valle MT, et al. Phenotypic and functional analysis of T cells homing into the CSF of subjects with inflammatory diseases of the CNS. J Leukoc Biol 2003;73: 584–90.
47. Teleshova N, Pashenkov M, Huang YM, Söderström M, Kivisäkk P, Kostulas V, et al. Multiple sclerosis and optic neuritis: CCR5 and CXCR3 expressing T cells are augmented in blood and cerebrospinal fluid. J Neurol 2002;249: 723–9.
48. Hanahan D, Weinberg R a. Hallmarks of cancer: the next generation. Cell 2011;144:646–74.
49. Holm JS, Funt SA, Borch A, Munk KK, Bjerregaard AM, Reading JL, et al. Neoantigen-specific CD8 T cell responses in the peripheral blood following PD-L1 blockade might predict therapy outcome in metastatic urothelial carcinoma. Nat Commun 2022;13:1935.
50. Kristensen NP, Heeke C, Tvingsholm SA, Borch A, Draghi A, Crowther MD, et al. Neoantigen-reactive CD8$^+$ T cells affect clinical outcome of adoptive cell therapy with tumor-infiltrating lymphocytes in melanoma. J Clin Invest 2022; 132:e150535.
51. Cloughesy TF, Mochizuki AY, Orpilla JR, Hugo W, Lee AH, Davidson TB, et al. Neoadjuvant anti-PD-1 immunotherapy promotes a survival benefit with intratumoral and systemic immune responses in recurrent glioblastoma. Nat Med 2019;25:477–86.
52. Osa A, Uenami T, Koyama S, Fujimoto K, Okuzaki D, Takimoto T, et al. Clinical implications of monitoring nivolumab immunokinetics in non–small cell lung cancer patients. JCI Insight 2018;3:e59125.
53. Duhen T, Duhen R, Montler R, Moses J, Moudgil T, De Miranda NF, et al. Co-expression of CD39 and CD103 identifies tumor-reactive CD8 T cells in human solid tumors. Nat Commun 2018;9:2724.
54. Simoni Y, Becht E, Fehlings M, Loh CY, Koo SL, Teng KWW, et al. Bystander CD8$^+$ T cells are abundant and phenotypically distinct in human tumour infiltrates. Nature 2018;557:575–9.
55. Wolfl M, Kuball J, Ho WY, Nguyen H, Manley TJ, Bleakley M, et al. Activation-induced expression of CD137 permits detection, isolation, and expansion of the full repertoire of CD8$^+$ T cells responding to antigen without requiring knowledge of epitope specificities. Blood 2007;110: 201–10.
56. Chow A, Uddin FZ, Liu M, Dobrin A, Nabet BY, Mangarin L, et al. The ectonucleotidase CD39 identifies tumor-reactive CD8$^+$ T cells predictive of immune checkpoint blockade efficacy in human lung cancer. Immunity 2023; 56:93–106.e6.
57. Kverneland AH, Chamberlain CA, Borch TH, Nielsen M, Mørk SK, Kjeldsen JW, et al. Adoptive cell therapy with tumor-infiltrating lymphocytes supported by checkpoint inhibition across multiple solid cancer types. J Immunother Cancer 2021;9:e003499.
58. Krishna S, Lowery FJ, Copeland AR, Bahadiroglu E, Mukherjee R, Jia L, et al. Stem-like CD8 T cells mediate response of adoptive cell immunotherapy against human cancer. Science 2020;370:1328–34.
59. Kortekaas KE, Santegoets SJ, Sturm G, Ehsan I, van Egmond SL, Finotello F, et al. CD39 identifies the CD4$^+$ tumor-specific T-cell population in human cancer. Cancer Immunol Res 2020;8:1311–21.
60. Voskoboinik I, Smyth MJ, Trapani JA. Perforin-mediated target-cell death and immune homeostasis. Nat Rev Immunol 2006;6:940–52.
61. Zheng C, Zheng L, Yoo JK, Guo H, Zhang Y, Guo X, et al. Landscape of infiltrating T cells in liver cancer revealed by single-cell sequencing. Cell 2017; 169:1342–56.e16.
62. Kim KH, Kim HK, Kim HD, Kim CG, Lee H, Han JW, et al. PD-1 blockade-unresponsive human tumor-infiltrating CD8$^+$ T cells are marked by loss of CD28 expression and rescued by IL-15. Cell Mol Immunol 2021; 18:385–97.
63. Kamphorst AO, Wieland A, Nasti T, Yang S, Zhang R, Barber DL, et al. Rescue of exhausted CD8 T cells by PD-1 targeted therapies is CD28-dependent. Science 2017;355:1423–7.
64. Hui E, Cheung J, Zhu J, Su X, Taylor MJ, Wallweber HA, et al. T cell costimulatory receptor CD28 is a primary target for PD-1-mediated inhibition. Science 2017;355:1428–33.
65. Woroniecka K, Chongsathidkiet P, Rhodin K, Kemeny H, Dechant C, Farber SH, et al. T-cell exhaustion signatures vary with tumor type and are severe in glioblastoma. Clin Cancer Res 2018;24:4175–86.
66. Davidson TB, Lee A, Hsu M, Sedighim S, Orpilla J, Treger J, et al. Expression of PD-1 by T cells in malignant glioma patients reflects exhaustion and activation. Clin Cancer Res 2019;25:1913–22.
67. Jenkins RW, Barbie DA, Flaherty KT. Mechanisms of resistance to immune checkpoint inhibitors. Br J Cancer 2018;118:9–16.
68. Hung AL, Maxwell R, Theodros D, Belcaid Z, Mathios D, Luksik AS, et al. TIGIT and PD-1 dual checkpoint blockade enhances antitumor immunity and survival in GBM. Oncoimmunology 2018;7:e1466769.
69. Raphael I, Kumar R, McCarl LH, Shoger K, Wang L, Sandlesh P, et al. TIGIT and PD-1 immune checkpoint pathways are associated with patient outcome and anti-tumor immunity in glioblastoma. Front Immunol 2021; 12:637146.
70. Cendrowski J, Mamińska A, Miaczynska M. Endocytic regulation of cytokine receptor signaling. Cytokine Growth Factor Rev 2016;32:63–73.
71. Saad E Ben, Oroya A, Rudd CE. Abstract 6528: anti-PD-1 induces the endocytosis of the co-receptor from the surface of T-cells: nivolumab is more effective than pembrolizumab. Cancer Res 2020;80:6528.
72. Lee AH, Sun L, Mochizuki AY, Reynoso JG, Orpilla J, Chow F, et al. Neoadjuvant PD-1 blockade induces T cell and cDC1 activation but fails to overcome the immunosuppressive tumor associated macrophages in recurrent glioblastoma. Nat Commun 2021;12:6938.
73. De Groot J, Penas-Prado M, Alfaro-Munoz K, Hunter K, Pei BL, O'Brien B, et al. Window-of-opportunity clinical trial of pembrolizumab in patients with recurrent glioblastoma reveals predominance of immune-suppressive macrophages. Neuro Oncol 2020;22:539–49.
74. Lu Y, Ng AHC, Chow FE, Everson RG, Helmink BA, Tetzlaff MT, et al. Resolution of tissue signatures of therapy response in patients with recurrent GBM treated with neoadjuvant anti-PD1. Nat Commun 2021;12: 4031.
75. Donia M, Hansen M, Sendrup SL, Iversen TZ, Ellebæk E, Andersen MH, et al. Methods to improve adoptive T-cell therapy for melanoma: IFN-γ enhances

anticancer responses of cell products for infusion. J Invest Dermatol 2013;133:545–52.
76. Dhatchinamoorthy K, Colbert JD, Rock KL. Cancer immune evasion through loss of MHC class I antigen presentation. Front Immunol 2021;12:636568.
77. Lee MY, Jeon JW, Sievers C, Allen CT. Antigen processing and presentation in cancer immunotherapy. J Immunother Cancer 2020;8:e001111.
78. Scheer M, Leisz S, Sorge E, Storozhuk O, Prell J, Ho I, et al. Neurofibromatosis *type 1* gene alterations define specific features of a subset of glioblastomas. Int J Mol Sci 2022;23:352.
79. Lobbous M, Bernstock JD, Coffee E, Friedman GK, Metrock LK, Chagoya G, et al. An update on neurofibromatosis type 1-associated gliomas. Cancers (Basel) 2020;12:114.
80. Zhang J, Caruso FP, Sa JK, Justesen S, Nam DH, Sims P, et al. The combination of neoantigen quality and T lymphocyte infiltrates identifies glioblastomas with the longest survival. Commun Biol 2019;2:135.
81. Hilf N, Kuttruff-Coqui S, Frenzel K, Bukur V, Stevanović S, Gouttefangeas C, et al. Actively personalized vaccination trial for newly diagnosed glioblastoma. Nature 2019;565:240–5.
82. Keskin DB, Anandappa AJ, Sun J, Tirosh I, Mathewson ND, Li S, et al. Neoantigen vaccine generates intratumoral T cell responses in phase Ib glioblastoma trial. Nature 2019;565:234–9.
83. Leko V, Cafri G, Yossef R, Paria B, Hill V, Gurusamy D, et al. Identification of neoantigen-reactive T lymphocytes in the peripheral blood of a patient with glioblastoma. J Immunother Cancer 2021;9:e002882.